

PALEOLIMNOLOGICAL RECORDS OF
ENVIRONMENTAL CHANGE PRESERVED IN
PALEO-LAKE MABABE, NORTHWEST BOTSWANA

By

JENNIFER L. GAMROD

Bachelor of Science in Geology

Southern Methodist University

Dallas, TX

December 2005

Submitted to the Faculty of the
Graduate College of the
Oklahoma State University
in partial fulfillment of
the requirements for
the Degree of
MASTER OF SCIENCE
May 2009

PALEOLIMNOLOGICAL RECORDS OF
ENVIRONMENTAL CHANGE PRESERVED IN
PALEO-LAKE MABABE, NORTHWEST BOTSWANA

Thesis Approved:

Dr. Anna Cruse

Thesis Adviser

Dr. Eliot Atekwana

Dr. Estella Atekwana

Dr. A. Gordon Emslie

Dean of the Graduate College

ACKNOWLEDGMENTS

I would like to thank the National Science Foundation (NSF) for funding this research through OISE grant #0217831, as well as the Ministry of Minerals and the Energy and Water Resources of the government of Botswana for granting the necessary permits to conduct this project. I would also like to thank Dr. Motsotse Modisi, Dr. Elisha Shemang, and Dr. Loago Molwalefhe of the University of Botswana for their support and contributions throughout this project. Thanks to Dr. Susan Ringrose and Dr. Huntsman-Mapila of the Harry Oppenheimer Okavango Research Center (HOORC) for making preparations for the field season as well as their contributions to the field work. Special thanks to Andy Foreman and Kristi Teter of Oklahoma State University for collecting the sediment samples and to Thebe for collecting samples for OSL dating. I would also like to thank the University of Botswana for providing logistical support and transportation for field work as well as the HOORC for providing vehicles for the field. Also, I would graciously like to thank the numerous individuals who came together in this collaborative project to provide technical and logistical support for this research, and without whom this project would not have been possible.

I would like to extend my sincerest thanks to my committee members Dr. Eliot Atekwana, Dr. Estella Atekwana, and Dr. Anna Cruse of Oklahoma State University (OSU) for all of your guidance, suggestions, and revisions. Thanks to Dr. Cruse for informing me of the project and Dr. Estella Atekwana for allowing me to become involved in the project. Special thanks to Dr. Eliot Atekwana for the countless hours you spent discussing every aspect of this work with me and the constant revisions that only improved my thesis. I would also like to thank Dr. Jim Puckette and Dr. Alex Simms for allowing me to use their equipment and always being available should I need them. I would also like to thank the OSU Geology Department for providing me funding in the form of a Skinner Fellowship during my stay at OSU.

Also, I would like to thank all of the faculty and staff of OSU and Southern Methodist University (SMU) for providing me a solid foundation in the geosciences. Especially, I would like to thank Dr. Neil Tabor of SMU for allowing me to conduct a senior thesis under his guidance, an invaluable experience which proved to help prepare me immensely for graduate school. I would also like to thank Dr. Kurt Ferguson and the Stable Isotope Laboratory at SMU for providing me the opportunity to work in the lab and become involved in research.

Thank you to the ConocoPhillips Corporation for their patience and understanding while I finished my degree and providing me a wonderful opportunity to begin working with them as a geologist. Additionally, I would like to thank the mentors I have had in the oil and gas industry, including Mike Shultz, Byron Davis, Bill Moulton, and John McCarty for preparing me for my future career.

I would also like to thank my friends Annie Drewry, Lauren Miller, Jared Rountree, Kyle Nelson, and Kristi Teter who understand all too well what a day of research is like when something does not go according to plan. Should you need to change the tubing on the particle size analyzer again please do not call me.

I would like to thank Brad Holland for all the support you have given me during this time and for always making the effort to drive up to spend time with me and help me in any way you could. I would also like to thank my parents and grandparents for always being supportive, and to my parents for helping me through school, supporting me, and always helping me in every way you could to allow me to better myself. I would especially like to thank my late-grandmother Hazel Gamrod for helping put me through school and teaching me to be independent. Above all though, I always knew no matter what I did you would always love me, support my decisions, and believe that I truly could do anything I put my mind to.

TABLE OF CONTENTS

Chapter	Page
I. INTRODUCTION.....	1
II. GEOLOGIC SETTING.....	3
2.1 Okavango River System	3
2.2 The Okavango Delta	3
2.3 The Mababe Depression	4
2.4 Paleo-lacustrine system.....	4
2.4.1 Lake Makgadikgadi Stage.....	4
2.4.2 Lake Thamalakane Stage.....	5
2.5 Tectonic Setting	5
III. METHODS	7
3.1 Field Work	7
3.1.1 Sample Collection.....	7
3.1.2 Lithologic Description	7
3.2 Sample Analyses.....	8
3.2.1 Magnetic Susceptibility	8
3.2.2 Particle Size Analysis	8
3.2.3 Inorganic Carbon and Organic Carbon Analysis.....	8
3.2.4 Metal Analysis	9
3.2.5 X-ray Diffractometry	9
3.2.6 Optically Stimulated Luminescence (OSL) Dating	9
IV. RESULTS.....	11
4.1 Zone 1: 560-485 cm.....	11
4.2 Zone 2: 485-375 cm.....	14
4.3 Zone 3: 375-280 cm.....	14
4.4 Zone 4: 280-240 cm.....	15
4.5 Zone 5: 240-195 cm.....	16
4.6 Zone 6: 195-145 cm.....	16
4.7 Zone 7: 145-75 cm.....	16
4.8 Zone 8: 75-0 cm.....	17
4.9 Metals.....	17

Chapter	Page
V. DISCUSSION	23
5.1 Tectonics and Lake Sedimentation	23
5.1.1 Evidence of Tectonism	23
5.1.2 Tectonic Alteration of Hydrology and Sedimentation.....	25
5.1.2.1 Sedimentation Pre-240 cm-depth.....	26
5.1.2.2 Sedimentation Pre-240 cm-depth.....	26
5.2 Paleoenvironmental History.....	27
5.2.1 Episode I (560-485 cm) > 65 ka	27
5.2.2 Episode II (485-375 cm) 65 ka to 41 ka	28
5.2.3 Episode III (375-240 cm) 41 ka to < 27 ka.....	29
5.2.4 Episode IV (240-0 cm) < 27 ka	30
5.3 Paleoclimate.....	33
VI. CONCLUSIONS	35
VII. FUTURE WORK	36
REFERENCES	37
APPENDICES	43
MabX	
Lithologic Section.....	A1-1
Physical Properties.....	A2-1
Carbonate and Organic Matter	A3-1
Metals Presented in Text.....	A4-1
Additional Metals.....	A5-1
Mab6	
Physical Properties.....	B1-1
Carbonate and Organic Matter	B2-1
Metals Presented in Text.....	B3-1
Additional Metals.....	B4-1
X-ray Diffractometry Results	C-1

LIST OF TABLES

Table	Page
1: Optically Stimulated Luminescence Dating	10

LIST OF FIGURES

Figure	Page
1a Location Map	6
1b Study Area	6
2 Particle Size Analysis Results.....	12
3 Physical Parameters	13
4 Transition Metals I.....	18
5 Transition Metals II.....	19
6 Alkali and Alkaline Earth Metals I.....	20
7 Alkali and Alkaline Earth Metals II.....	21
8 Conceptual Model.....	32

CHAPTER I

INTRODUCTION

The Middle Kalahari of northwestern Botswana (*sensu* Passarge, 1904) is a structural depression that contains lake basins which preserve a record of environmental change and tectonic activity (e.g., Huntsman-Mapila et al., 2006; Thomas and Shaw, 1991; Thomas and Shaw, 2002). Regional and local climate shifts can result in the environmental changes observed in these basins. Currently, the Middle Kalahari region is a semiarid environment that had a wetter climate in the past that caused the development of lakes. In addition to local rainfall, the lakes also receive water from rivers such as the Okavango and Kwando Rivers, which drain tropical watersheds in the Angolan highlands. Therefore, the lake sediments are derived from local and distal sources. Tectonic activity associated with the south-westerly propagating Okavango Rift (e.g., Modisi et al., 2000) also contributes to environmental changes by altering the landscape and hydrology. For example, faulting along the Okavango rift interrupted the flow of the Okavango River causing sedimentation that formed the Okavango Delta, which is actually a 25,000 km² alluvial fan (McCarthy et al., 2002). Development of the vast Okavango Delta has altered the topography and hydrologic conditions of the region, which likely changed lacustrine hydrologic and sedimentary budgets. Lake sediments thus represent a unique setting that may preserve a record of local and regional climate change and rift tectonics.

Early research on environmental change in the Middle Kalahari region focused on describing landforms (e.g., Passarge, 1904; Wellington, 1955; Grove, 1969) but, more recently these investigations have centered on understanding geomorphological features such as beach ridges around lacustrine systems such as the Mababe Depression, Lake Ngami, and the Makgadikgadi Pans (Grove, 1969; Grey and Cooke, 1977; Shaw, 1985). Efforts to understand the timing of beach ridge formation have been improved by the acquisition of age dates through the use of radiocarbon (¹⁴C), thermoluminescence (TL), and optically stimulated luminescence (OSL) dating techniques (e.g., Cooke and Verstappen, 1984; Shaw, 1985; Burrough et al., 2007; Burrough and Thomas, 2008; Ringrose et al., 2008; Burrough and Thomas, 2009). Recent studies of shorelines around Lake Ngami (Shaw et al., 2003; Burrough et al., 2007) and the Mababe Depression (Burrough and Thomas, 2008), however, are providing new insights on the role of climate in contributing to lake highstand events and the development of shorelines in the region.

Investigations of the local climate have been conducted on deposits in Drotsky's Cave in the Kwihabe Hills of northwest Botswana (Cooke, 1975; Cooke and Verhagen,

1977). Climate records from the cave deposits show episodes dominated by wet and dry conditions in the local and regional climate, as well as cyclic climatic conditions (Cooke, 1975; Shaw and Cooke, 1986). Although northwest Botswana is currently a semi-arid environment, these studies indicate that wet periods occurred in the past. Sinter deposition, which reflects high local rainfall, occurred at 45-37 ka, 34-29 ka, 16-13 ka, 2 ka, and 750 years ago (Cooke and Verhagen, 1977; Shaw and Cooke, 1986). These episodes of sinter deposition correspond to wet episodes from 17-14 ka, which includes a possible regional event at 16 ka, 4.35 ka, and 2 ka, that were identified by cave studies conducted by Cooke (1975).

Tropical climatic signals have been recognized in sediments from Etosha Pan of Namibia (Brook et al., 2007) where shoreline features along the pan correspond to times of an overall wetter climate during the Holocene. The headwaters of the Okavango River receive rainfall in the same area of the Angolan highlands that is responsible for inflow to the Etosha Pan, thus, shifts in the tropical climate patterns that are observed in the pan should also occur in the sedimentary records of the Middle Kalahari lake deposits. In addition to local climate shifts recorded in cave deposits, climatic variations occurring in the tropical Angolan highlands influence river flow into the lakes and, also, affect the lacustrine hydrology and sedimentation in the Middle Kalahari basin.

Studies on beach ridges and caves can be useful in deciphering the climatic history of the area; however, they cannot provide a complete record of both climatic and tectonic events with the same resolution as sediments collected within the lake basins. Beach ridges represent only the most recent occurrence of a lake highstand, because, by their very nature, ridges at lower levels could be reworked during subsequently higher lake levels, thus, past events are lost from the sedimentary record (Burrough and Thomas, 2009). Similarly, cave studies can provide a continuous record of local and regional climate change, but they cannot be used to decipher the influence of tectonic processes on hydrology or sedimentation. Unlike lakes in semi-arid and arid environments that only derive sediments from local sources during locally wet climatic episodes, lakes of the Middle Kalahari receive water and sediment input from tropical environments such as the Angolan highlands. During dry local conditions, sediments may only be derived from distal sources; however, lake levels may still be affected by conditions such as evaporation that could affect lake productivity and chemical sedimentation. Sediments from the Kalahari lake basins, therefore can provide the most complete record of local and regional climate influence on the region and can provide insight into the timing of tectonic events based on changes in sedimentation that are preserved in the lake sediments.

Geochemical proxies measured from sediments within Lake Ngami (Huntsman-Mapila et al., 2006), at the distal end of the Okavango Delta, show similar results to climate variations preserved from beach ridge and cave studies. Additionally, the study also revealed a possible tectonic control on the sedimentation.

In this study, sediment samples were collected from within the Mababe Depression and analyzed for particle size distribution, high frequency magnetic susceptibility, carbonate, organic matter, and metal content. Each of these data sets were examined in combination to determine how environmental changes related to climate and tectonics are recorded in lake sediments.

CHAPTER II

GEOLOGIC SETTING

2.1 Okavango River System

The Cubango and Cuito Rivers are major tributaries that drain the tropical Angolan highlands and come together to form The Okavango River (Fig. 1a). The Cubango River, in the western Angolan catchment, is affected by variations in the Atlantic equatorial westerlies, while the Cuito River, to the east, responds to tropical lows in Indian Ocean Easterlies, both of which are affected by the position of the Intertropical Convergence Zone (ITCZ) (Huntsman-Mapila et al., 2006). Rainfall in the catchment of Angola can have a profound impact on the Okavango River because it is sourced from this area. It is these rivers that supply the majority of water to the Okavango Delta, an average of 9200 million m³ yr⁻¹, but this value varies considerably each year (McCarthy and Ellery, 1998).

2.2 The Okavango Delta

The Okavango River enters the Makgadikgadi-Okavango-Zambezi (MOZ) rift depression (Ringrose et al., 2005) of northern Botswana through a narrow swamp, known as the Panhandle, that has developed along a fault trending NW-SE (Gumbrecht et al., 2001), before spreading out into a series of permanent and seasonally flooded swamps. Although the catchment for the Okavango Delta is sourced in the tropics, the “delta” is located in the semi-arid environment of the Middle Kalahari region (*sensu* Passarge, 1904; Fig. 1a). At over 25,000 km², the Okavango Delta is one of the world’s largest alluvial fans and has been characterized as a losimean, or, low sinuosity-meandering fan (Stainstreet and McCarthy, 1993). Topographic relief across the fan is very low, with gradients averaging only 1:3550 (Gumbrecht et al., 2001).

Local precipitation also contributes an average of 6140 million m³ yr⁻¹ of water to the Okavango Delta (McCarthy et al., 1998). Rainfall and river flow in the Okavango Delta maintains about 4,000 km² of permanent swamps and up to 12,000 km² of seasonal swamps (McCarthy et al., 2002). Water from the catchment along with local flow carries ~209,000 tonnes of sediment, of which approximately 77% is bedload material (McCarthy et al., 2002). Total dissolved solids entering the Okavango Delta contribute another 450,000 tonnes of material, but, only ~30,000 tonnes leave as outflow (McCarthy and Metcalfe, 1990). In contrast, almost no sediment leaves the Okavango Delta and ~96% of inflow to the delta is lost to evapotranspiration, while the remainder leaves as

surface or groundwater flow (Dincer et al., 1979). Due to the exceedingly high evapotranspiration rates across the Okavango Delta, sodium salts, such as trona, accumulate on the fan surface (McCarthy et al., 1986; McCarthy and Metcalfe, 1990). Calcium carbonate and silica are the most abundant chemical sediments accumulating on the fan each year, and, chemical sedimentation results in 250,000 tonnes of accumulation compared to ~40,000 tonnes of clastic materials (McCarthy and Metcalfe, 1990).

2.3 The Mababe Depression

The Mababe Depression is a heart-shaped feature that lies at the distal end of the Okavango Delta (~18° S to 19° S, 24° E to 24°30' E), and is ~90 x 50 km at its' widest dimensions (Fig. 1a). Inflow to the Mababe Depression occurs where the Khwai River joins the channel of the Thamalakane River to form the Mababe River at the southern end of the depression, which supplies water to the Mababe Swamp (Fig. 1b). Along the northwestern margin, flow from the Okavango Delta moves east through the Selinda Spillway before joining flow from the Kwando-Linyanti River and flow down the Savuti channel into the Mababe Depression, where it terminates in the Savuti Swamp (Fig. 1b). Inflow from the Savuti, however, is infrequent at present (Shaw, 1988), but, greater volumes of water once flowed through the channel, as it is presently an underfit channel (Shaw, 1985). Rivers in the northeast, such as the Ngwezumba, Kashaba, and Gautumbi can also provide water to the Mababe Depression during times of high local rainfall (Fig. 1b).

The Magikwe Ridge, on the western side of the basin, is a remnant shoreline feature located to the southeast of the Linyanti Fault. Bounding Mababe to the southeast is the northeast-southwest striking Thamalakane Fault. Scholz et al. (1976) noted that the south-eastern edge of the depression is nearly linear along the strike of this fault and suggested that the Mababe Depression is fault-bound. The Thamalakane Fault serves as a link between the Mababe Depression and Lake Ngami, located to the southwest. Low gradient channels that flow alongside the Thamalakane Fault can connect Lake Mababe and Lake Ngami during times of high lake levels. Another sub-basin connected to Mababe and Ngami is the Makgadikgadi Pans towards the southeast, which is linked by the Boteti River to the Thamalakane River.

2.4 Paleo-lacustrine System

2.4.1 Lake Makgadikgadi Stage

Evidence that the Mababe, Ngami, and Makgadikgadi subbasins were once connected is apparent via a series of beach ridges seen along each basin at 945 m above sea level that suggest the coalescence of these basins during the Quaternary (Grove, 1969; Grey and Cooke, 1977; Shaw, 1985; Shaw, 1988). Beach ridges, or shoreline features that are relict wave or wind-built ridges (Otvos, 2000), at the 945 m level represent the formation of Paleo-lake Makgadikgadi. Geomorphological evidence from beach ridges indicate that this lake-stage would have encompassed an area of ~60,000 km² (Grey and Cooke, 1977) but, possibly as much as 120,000 km² (Thomas and Shaw,

1991). Based on ^{14}C dating the Makgadikgadi stage was last present at ~40,000 to 35,000 BP, but may be as older than 52,000 BP (Cooke and Verstappen, 1984).

2.4.2 Lake Thamalakane Stage

Lake Thamalakane (Shaw, 1988) is identified by a series of shoreline features around the Mababe and Ngami basins at 936 m elevation, which is indicative of the coalescence of the two lakes around the Thamalakane axis (Shaw and Cooke, 1986). Burrough and Thomas (2008) document the existence of Lake Thamalakane using OSL dating methods. Shaw et al. (1988) postulated that outflow along the Boteti River may have resulted in a lake level of 920 m in the Makgadikgadi basin that coincided with the 936 m stage inferred in Mababe Depression and Lake Ngami. Estimates on the size of Lake Thamalakane based on SRTM data suggest a total surface area of ~32,000 km² (White and Eckardt, 2006).

At least two periods of this lake level are identified by Shaw (1985) based on ^{14}C dates of pedogenic calcretes which date the events from 17,000 to 12,000 BP and ~2,000 BP with episodes of low lake levels up to 932 m at 6,000 BP. Burrough and Thomas (2008) identified other possible Thamalakane stages between ~38,000 to 35,000 BP in the Mababe Depression that correspond to the formation of the Dautsa Ridge in Lake Ngami between 38,000 and 30,000 BP (Burrough et al., 2007). Another Thamalakane stage occurred as a transgressive ridge building episode between ~8,000 to 5,000 BP and can be observed on the western shorelines of the Mababe Depression (Burrough and Thomas, 2008).

2.5 Tectonic Setting

The Mababe Depression is situated within the Okavango Rift Zone (ORZ), which locally extends from the Gomare Fault in the Panhandle area to the Kunyere and Thamalakane Faults that mark the SE boundary of the rift (Modisi, 2000; Fig. 1a). The ORZ is at the terminus of the southwestern branch of the East African Rift System (EARS) and represents a segment of the rift system that formed in the Quaternary (Modisi et al., 2000; Kinabo et al., 2007). The northeast-southwest trending southwestern branch, however, is considerably younger than the eastern and western branches of the EARS system, which are >15 Ma and <15 Ma years, respectively (Kampunzu et al., 1998).

Tectonic activity observed from Lake Tanganyika to central Botswana led to the interpretation by Fairhead and Girdler (1969) that the area was part of an incipient rift zone. Scholz et al. (1976) noted that the Okavango Delta was situated in a 150 km wide, possibly asymmetric graben, which is believed to be a foundation of a developing continental rift (Scholz and Contreras, 1998). While other works have examined graben development in the area (e.g. Modisi, 2000) it is unclear what stage of development the ORZ is in. Kinabo et al. (2007) postulate that the area is part of a synformal depression to early half-graben stage, but, McCarthy et al. (2002) suggest that the area is a depression formed by uparching and upthrow along northeast-striking faults and not an incipient rift graben.

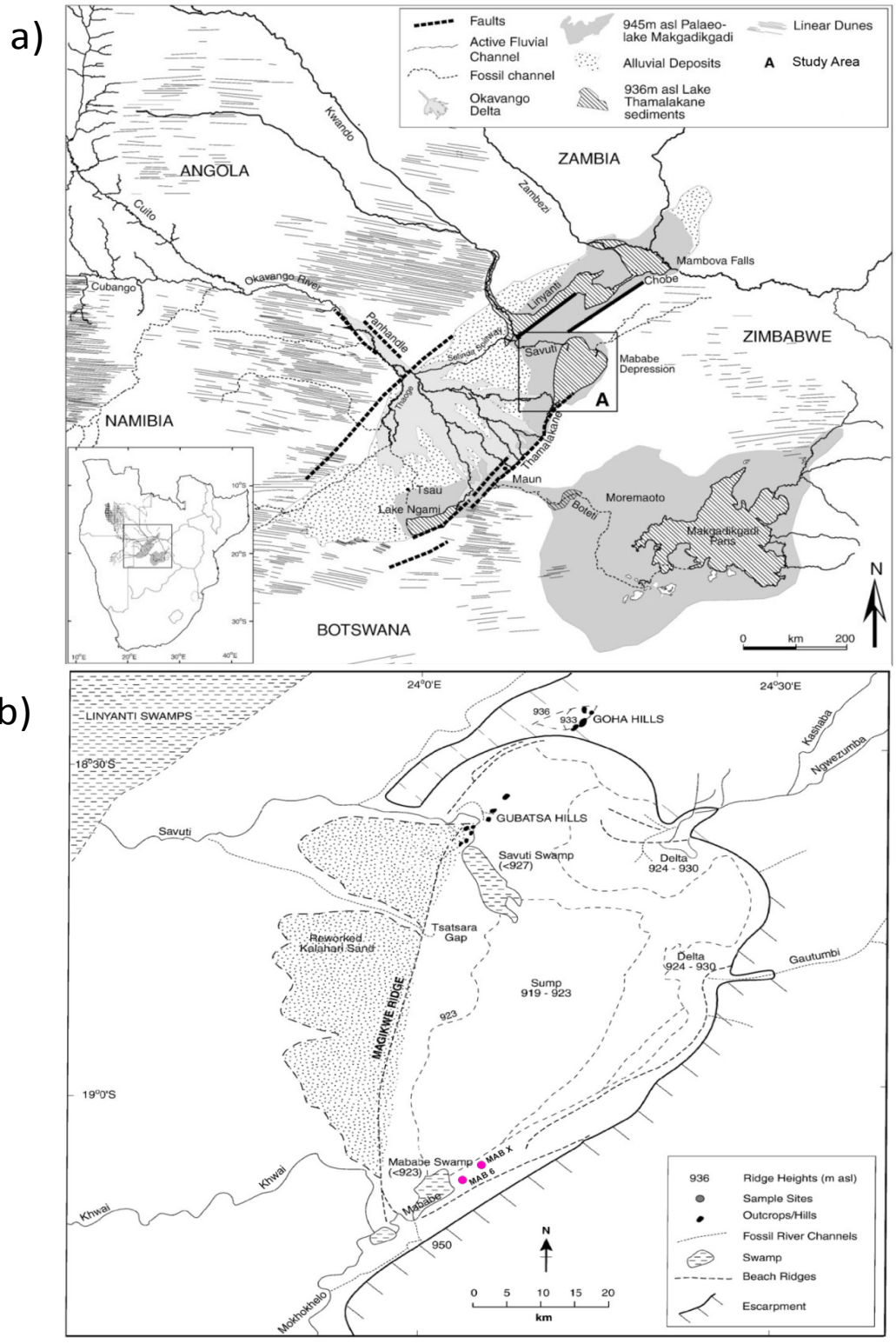


Figure 1 a) Map showing the Okavango, Kwando, and Zambezi River systems. Insert A shows the study area in more detail in Figure 1b) Map of the Mababe Depression. Sample locations Mab X and Mab 6 are shown (Modified from Burrough and Thomas, 2008).

CHAPTER III

METHODS

3.1 Field Work

3.1.1 Sample Collection

Samples were collected from two trenches, MabX (19°S, 06'19.8", 24°E, 05'04.8") and Mab6 (19°S 07'42.2", 24°E 03'28.6"), located in the southwest portion of the Mababe Depression, near the terminus of the Mababe River (Fig. 1b). Trenches were constructed by an excavator. Sediments observed on the walls of the trenches were described prior to sampling. MabX was sampled every five centimeters to a depth of 5.6 m, aside from intervals 545 and 555, which were not collected due to sampling difficulties. Mab6 was sampled every 20 cm to a depth of 4.4 m. Sediment from each sampled interval was stored in a plastic bag and transported to the laboratory, where 50 g of sample was crushed with a mortar and pestle and stored in scintillation vials.

During sample collection five intervals were selected for OSL (Optically Stimulated Luminescence) dating. Four samples from MabX at 45 cm, 135 cm, 380 cm, and 500 cm-depth, respectively, were collected as boulder-sized samples. These samples were then protected from exposure to sunlight by wrapping the samples in layers of aluminum foil, and were then returned to the lab for dating.

3.1.2 Lithologic Description

Sediments from both MabX and Mab6 consist mainly of silty diatomites, diatomaceous clayey-silts, clayey-silts, and organic-rich sediments. Clay layers, silts with clay clasts, clayey-silty diatomites, clayey diatomites, sands, sandy clay silts, and silty diatomites also occur in MabX (see Appendix A1). Layers observed from 560-240 cm appear cyclic in nature with the exception of 375 cm to 335 cm-depth. Below 485 cm in MabX the lithology is dominated by sandy-clay silts from 560 cm to 530 cm and 505 cm to 485 cm. Silty diatomites are present in the section from 530 cm to 520 cm. Diatomite layers dominate the section from 485 cm to 375 cm-depth, but show variability in color that includes light-brown, light-gray, white, light-tan, and white-gray diatomites. A clayey-silt layer is present from 370 cm to 350 cm-depth and is overlain by a 15 cm-thick sand layer. Diatomaceous layers occur again from 335 cm to 240 cm. Clayey-silty diatomite is present from 335 cm to 320 cm and is overlain by 20 cm of diatomaceous clayey silt that is interbedded with 5 cm of brown diatomite. At 300 cm to 240 cm-depth

light-tan and white-gray diatomites are observed in the section, except for a 5 cm-thick clayey-silt at 245 cm.

Diatomite layers are noticeably absent above 240 cm, except for a 15 cm-thick interval of light-brown gray diatomite overlain by a light-brown diatomite from 145 cm to 120 cm-depth. Lithologies above 240 cm are non-cyclic in nature and are dominated by diatomaceous clayey-silts, silts with clay clasts, and organic-rich sediments. Diatomaceous clayey-silt occurs from 240 cm to 195 cm-depth and is overlain by a silt with clay clasts, with clasts increasing upwards in abundance, from 195 cm to 155 cm-depth. A clay lens 10 cm-thick overlies the silt with clay clasts and is overlain by diatomite layers from 145 cm to 120 cm-depth. Another diatomaceous clayey-silt is present at 120 cm to 110 cm-depth and is overlain by a 35 cm-thick clayey silt. Capping the section is an interval of organic-rich sediments. At 75 cm to 50 cm-depth is an organic-rich silt, followed by an organic-rich clayey-silt to 25 cm-depth. Within the top 25 cm is another organic-rich silt layer.

3.2 Sample Analyses

3.2.1 Magnetic Susceptibility

Variable concentrations of magnetizable materials such as ferromagnetic, paramagnetic, and diamagnetic minerals present in sediments affect the strength of magnetism in a given sample (Ellwood et al., 2004). Magnetic susceptibility (MS) is a technique used to determine the concentration of magnetizable materials in a sample. High frequency magnetic susceptibility (X_{hf}) was measured for each sample collected from the MabX and Mab6 trenches using a Bartington MS2 magnetic susceptibility meter with an MS2B dual frequency sensor. MS values were measured on approximately 10 g samples and reported in terms of mass, due to the ease and efficiency in obtaining high precision measurements by this method (Ellwood et al., 2008)

3.2.2 Particle Size Analysis

Particle size analysis was performed using laser diffractometry on a Cilas1180 particle size analyzer with a detection range of 0.04 to 2500 μm . Approximately 100 ml of deionized water was added to ~10 g of uncrushed sample and dish detergent was used as a dispersal agent. Samples were kept undisturbed for 24 hours before being mixed by a magnetic stirrer and introduced to the Cilas1180 by pipette analysis. Target obscurations of 15-20% were obtained for all samples. Each sample was run for 120 s with ultrasonics to break up any agglomerates (Sperazza et al., 2004). Samples were then measured five times, without ultrasonics, and analyzed using the Fraunhofer theory. Grain size distribution statistics were calculated according to the method of Folk and Ward (1957).

3.2.3 Inorganic Carbon and Organic Carbon Analysis

Total inorganic carbon (TIC) and total organic carbon (TOC) concentrations were determined using a CM5014 Coulometer equipped with a CM5130 Acidification Module

and a CM5300 Furnace Module. For TIC analysis, a pre-weighed sample was reacted with 2N H₂SO₄ to release CO₂, which was titrated electronically. Total carbon (TC) was determined by combusting a pre-weighed sample in the furnace module at 950°C. TOC was calculated by the difference between TC and TIC values.

3.2.4 Metal Analysis

Approximately 100 mg of sample were dissolved using aqua regia (3:1 mixture of HCl:HNO₃) in a microwave digestion unit. Dissolution in aqua regia is a widely used method that can yield recoveries of metals in sediments that range from 89 to 110% (Sastre et al., 2002). Microwave-assisted digestion was performed using a MarsXpress microwave oven. After digestion, samples were evaporated and reconstituted with 20 ml of 2% HNO₃ three times. After the final evaporation and reconstitution, the samples were cooled and filtered through a 45 µm Whatman filter into acid pre-washed polyethylene bottles and diluted to a total volume of about 60 ml with 2% HNO₃. Metals were measured using a PerkinElmer Optima 2100DV inductively coupled plasma optical emission spectrometer (ICP-OES).

3.2.5 X-ray Diffraction

Two samples from MabX (265 cm and 305 cm) and two samples from Mab6 (200 cm and 320 cm) were selected for bulk mineralogy runs on a Philips PW 1830 X-ray diffractometer (XRD) equipped with a Cuα radiation source. Samples were powdered and run from 5-40° at 2θ per minute. Subsequently, clays were extracted according to the methods of Kittrick and Hope (1963). Extracted samples were then run from 2-30° at 2θ per minute to determine clay mineralogy.

3.2.6 Optically Stimulated Luminescence (OSL) Dating

After samples were collected in the field they were returned to the Radiation Dosimetry Laboratory at Oklahoma State University for processing. Samples were sieved and treated with HCl and H₂O₂ to remove carbonates and organic matter, respectively, before a 50-minute treatment with HF to remove the outer portion of the grains that were affected by radiation. Sediments were then retreated with HCl and quartz grains were separated. Water content of the samples was determined based on the weight difference between the wet and dried sample. Water content for all the samples ranged from 1% to 3% but, an average water content of 10% was assumed for the samples because they were deposited in a lacustrine environment. Following this, samples were stored in air-tight containers for four weeks before Th, U, and K concentrations were measured according to the conversion factors of Adamiec and Aitken (1998).

The natural equivalent dose (D_e) is determined by comparison of the natural luminescence signal with the one obtained from the response of samples to a known radiation exposure in the laboratory. The intensity of the luminescence signal is proportional to that of the radiation dose and is reported in units of Gray (Gy). Measurements were conducted using a Risø TL/OSL-DA-15 reader, Risø National

Laboratory, with a bialkali PM tube (Thorn EMI 9635QB) and Hoya U-340 filters (290-370 nm) with a built-in $^{90}\text{Sr}/^{90}\text{Y}$ beta source. Blue LEDs (470 nm) were used for optical stimulation.

The dose rate of the samples that is attributed to cosmic radiation is dependent on the geographical location of the sample site (19°S, 24°E, 930 m asl) and was calculated according to the methods of Prescott and Stephan (1982) and Barbouti and Rastin (1983). A final age was then determined based on the equivalent dose divided by the dose rate. Equivalent dose, dose rate, and determined age are reported in Table 1.

Table 1: Results of Optically Stimulated Luminescence Dating

Sample	Dose ¹ (Gy)	Dose Rate ² (Gy/ka)	Age ³ (ka)
MabX 45	21.6 ± 1.3	1.847 ± 0.087	11.70 ± 0.90
MabX 135	35.9 ± 2.0	1.332 ± 0.061	27.0 ± 2.0
MabX 380	60.7 ± 2.6	1.469 ± 0.070	41.3 ± 2.7
MabX 500	147.3 ± 7.7	2.27 ± 0.12	64.8 ± 4.7

¹Equivalent Dose

²Dose Rate

³Age in thousands of year

CHAPTER IV

RESULTS

Zones are defined for the sedimentary section based on multi-proxy data sets to delineate events that are significant in altering sediment type and relative grain size distribution of paleo-lake Mababe. Zones are determined based on changes in trends of the percent silt and clay content (Fig. 2) and X_{hf} (Fig. 3), assuming, the variations could be attributed to processes that control lake water levels. Sorting and skewness (Fig. 2) of the samples, as well as carbonate and organic matter content (Fig. 3) were used to further identify the zones. After zones were identified, metal results (Figs. 4-7) were used to support the established zones and provide further insight on processes affecting sedimentation in the Mababe Depression.

4.1 Zone I: 560-485 cm

Zone I consists of a 30 cm-thick sandy clay silt layer at the base, which is overlain by 5 cm-thick layers of silty diatomite and clayey diatomite, followed by a 15 cm-thick clayey silt. The upper 20 cm of this zone is marked by another sandy clay silt layer. Sediments in the basal sandy clay silt average 4% sand in the lower part of the layer before increasing to 10% near the top, and, then decreasing to 3% at the top of the layer. Sand content in the diatomaceous and the clayey silt layers is less than 0.5%. Within the sandy clay silt layer at the top of the zone, sand increases to 12% before declining to 4% at the top of the zone. In the basal sandy clay layer, silt remains nearly constant while clay content decreases from 19% to 14% near the top of the unit, due to increase sand content. The clay content remains at ~15% in the silty diatomite layer. Within the clayey diatomite, however, clay increases to 22%, and then to 26% at the base of the clayey silt unit but varies from 18-20% throughout the upper sand clay silt layer. The decrease in silt and clay in the upper sandy clay silt layer corresponds to increase in sand to about 10%.

Sediments in Zone I are poorly sorted, although to slightly different degrees in each layer, with an average SD value of 1.6 ϕ within the basal sandy clay silt layer and a lower SD of 1.5 ϕ within the diatomaceous and clayey silt layers, but the upper sandy clay silt layer is the most poorly sorted. The skewness of sediments is also highly variable throughout this zone. The basal sandy clay silt is coarsely-skewed to finely-skewed, while the diatomaceous and clayey silt layers vary between finely and very finely-skewed and the upper sandy clay silt is near-symmetrical.

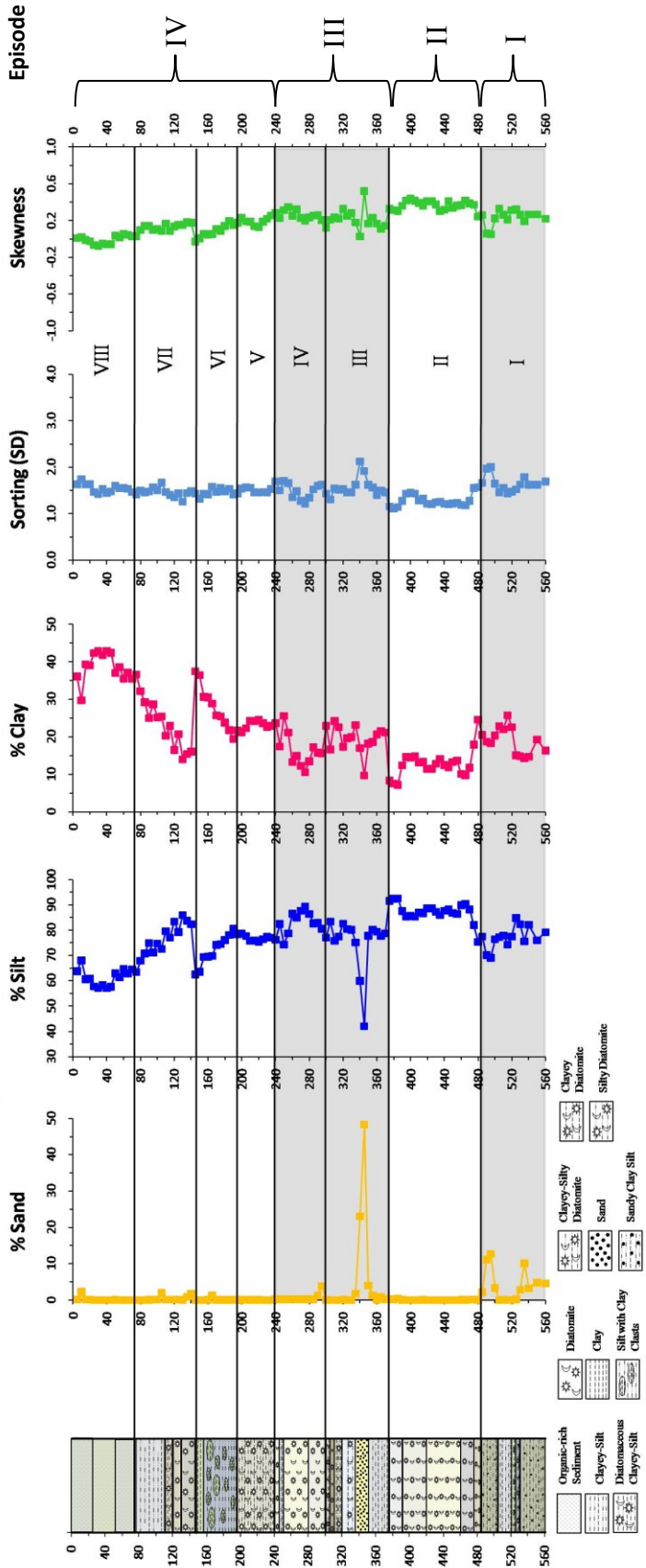


Figure 2: Particle size analysis results given as percent sand, silt, and clay, along with grain sorting and skewness, compared to the lithologic section.

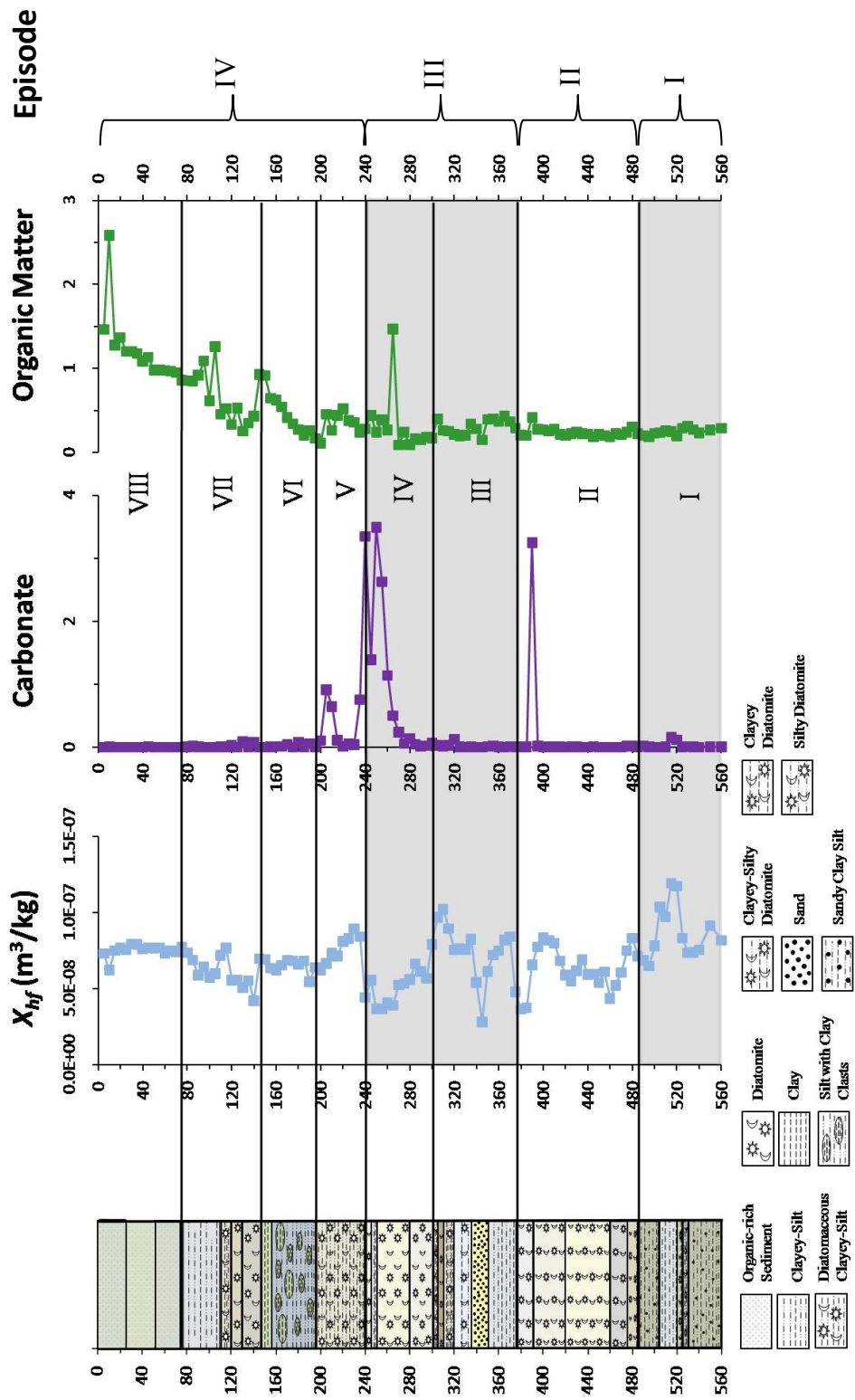


Figure 3: High frequency magnetic susceptibility, carbonate, and organic matter results compared to the lithologic section.

X_{hf} values in the basal sandy clay silt ($\sim 7 \times 10^{-8}$ m³/kg) decrease slightly in the silty diatomite layer and increase markedly within the clayey diatomite to a maximum value of 1.2×10^{-7} m³/kg in the clayey silt layer. The X_{hf} decreases again to $\sim 7 \times 10^{-8}$ m³/kg in the upper sandy clay silt layer. Carbonate content is generally low (<0.1%) and remains low in the zone except for slight increase to 0.4% in the base of the clayey silt layer. This increase in carbonate corresponds to the highest X_{hf} values and Al and Fe content in the clayey silt layer. The organic matter content is low and nearly constant at 0.1% throughout the zone.

4.2 Zone II: 485-375 cm

Zone II consists of 110 cm of diatomaceous layers that display subtle variations in color. Light-brown diatomite marks the basal 10 cm of the zone and is overlain by a 15 cm-thick light-gray diatomite, followed by a 35 cm interval of white diatomite, and a 25 cm-thick light-tan diatomite. The upper layer of this unit is a 15 cm-thick white-gray diatomaceous bed. Sand accumulation in Zone II sediments is < 0.1%, and, no measureable sand is recorded within the white diatomite. Silt content, however, shows a pronounced increase from $\sim 75\%$ to 90% and clay decreases from 25% to only 10% from the base of the zone to the top of the light-gray diatomite. Silt averages of $86\text{-}87\%$ in the white diatomite and the overlying light tan diatomite. Clay averages $10\text{-}14\%$ across the white diatomite layer until the base of the light-tan diatomite layer, where clay steadily increases to over 14% . At 435 cm-depth, in the white diatomite layer, clay increases to 14% and silt decreases to 86% . The white-gray diatomite that marks the top of the unit has a silt content of 92% and a markedly lower clay content of $\sim 7.5\%$.

Within the zone, sediments are poorly sorted and average 1.25Φ throughout the light-gray, white, and white-gray diatomite layers. Poorer sorting is observed in the light-brown and light-tan diatomites with averages of 1.6Φ and 1.5Φ , respectively. Skewness also changes from finely-skewed in the light brown diatomite to very finely-skewed across the light-gray diatomite. Sediments trend toward finely-skewed within the lower white diatomite, before becoming increasingly very finely-skewed within the rest of the layer. Another trend toward very finely-skewed occurs in the light-tan diatomite, before trending toward finely-skewed sediments in the upper light-tan and white-gray diatomites at the top of the zone.

X_{hf} values peak at 8×10^{-8} (m³/kg) at the base of the section in the light brown diatomite and decline to 4×10^{-8} (m³/kg) at the top of the light-gray diatomite. X_{hf} values in the white diatomite average 5.5×10^{-8} (m³/kg). In the light-tan diatomite, X_{hf} increases again to highs of 8×10^{-8} (m³/kg) before declining to $< 3.5 \times 10^{-8}$ (m³/kg) in the white-gray diatomite layer, where it remains nearly constant. Carbonate and organic matter maintain average values of 0.1% and 0.3% , respectively, throughout this zone. At 390 cm-depth, however, carbonate spikes to $> 3\%$, which coincides with an increase in organic matter to $\sim 0.4\%$.

4.3 Zone III: 375-280cm

Zone III consists of a 20 cm-thick clayey silt overlain by 15 cm of sand. Diatomaceous sediments overly the sand and include a clayey-silty diatomite for 15 cm,

overlain by a diatomaceous clayey silt that contains a 5 cm-thick interbed of brown diatomite, that caps the zone. The basal clayey silt has sand values of < 0.5% that increase to 4% upward in the bed, and silt values average 80%. Almost 50% sand is obtained at the base of the sand layer, which then decreases to ~2% at the top of the layer. As sand content increases across the layer, both silt and clay decrease proportionally, with silt decreasing to 42% and clay decreases to ~10%. The top of the sand unit marks a transition into a clayey-silty diatomite layer that contains negligible sand content and silt and clay values that average 81% and 19%, throughout the upper diatomite layers.

Most units within the zone are poorly sorted and have an average SD of ~1.5 Φ , however, the sandiest interval is very poorly sorted (SD=2.1 Φ). Grains are finely-skewed throughout the clayey silt but are very finely-skewed within the sand before becoming near-symmetric within the upper sand. Sediments that border between finely-skewed and very finely-skewed occur within the clayey-silty diatomite, before becoming finely-skewed throughout the rest of the zone.

Within Zone III, distinct patterns in X_{hf} values that range from 8.5×10^{-8} (m^3/kg) to 6×10^{-8} (m^3/kg) observed in the clayey silt. X_{hf} values ranges from 2×10^{-8} (m^3/kg) at the base of the sand layer to over 8×10^{-8} (m^3/kg) at the top of the layer. Steady X_{hf} values occur throughout the clayey-silty diatomite layer, with an average of 7.5×10^{-8} (m^3/kg). Increasing X_{hf} is seen within the bottom portion of the diatomaceous clayey silt, but, the brown diatomite interval marks the beginning of a decrease from 1×10^{-7} (m^3/kg) to 7.5×10^{-8} (m^3/kg) throughout the remainder of the zone. Organic matter is nearly constant at ~0.4% in the silty-clay layer, and displays subtle increases to 0.3% and 0.4% within the sand and overlying diatomite layers. Carbonate values remain low (< 0.1%) until the clayey-silty diatomite layer, when values increase to ~0.3%.

4.4 Zone IV: 280-240 cm

Zone IV consists of a light-tan diatomite layer 20 cm-thick, followed by a 40 cm-thick white diatomite layer with a 5 cm-thick clayey silt layer interbedded at 245 cm. The base of the light-tan diatomite represents a sand accumulation of ~4%, but, sand is < 0.3% across the remainder of the zone. Silt increases from 80% at the base of the light-tan diatomite to 86% at the top of the layer. Clay decreases from 15% at the base of this bed to 10% at the top of the layer, followed by a continuous increase to ~20%, except for in the clayey silt layer where clay decreases to ~17%.

Poor sorting occurs throughout this zone. Sorting at the base of the zone averages ~1.75 Φ but, becomes more poorly sorted throughout the light-tan diatomite, before increasing to the top of the zone. In the lower light-tan diatomite, basal portions of the overlying white diatomite, and the upper 10 cm of the zone, sediments are finely-skewed, but become very finely-skewed from 270 to 250 cm, with the exception of the finely-skewed interval at 260 cm.

Magnetic susceptibility increases slightly within the light-tan diatomite from 5.75×10^{-8} to 7×10^{-8} (m^3/kg) before decreasing across the bottom 20 cm of the white diatomite from 5.5×10^{-8} to 3.5×10^{-8} (m^3/kg). Zone IV is characterized in large part by increasing carbonate values. Carbonate values increase from the base of the zone to 3.5%, except for the clayey silt layer that declines 1.3%. Organic matter in this zone

increases continually to 0.5% between the white diatomite layer and the top of the zone, with a spike of 1.5% at 265 cm.

4.5 Zone V: 240-195 cm

A diatomaceous clayey-silt layer 45 cm-thick comprises Zone V. No significant variation in sand (0.1%) is observed in the unit. Silt content averages 76% and, clay 24%, for the bottom 30 cm of the layer before silt steadily increases to 78% and clay decreases to 21%. The bottom of the zone is poorly sorted with a SD of 1.45 Φ that increases to 1.55 Φ in the upper portion of the zone. Sediments are finely-skewed throughout the zone but, show better sorting across the bottom 25 cm of the zone and become increasingly finely-skewed in the upper portion of the zone.

X_{hf} steadily decreases across the entire zone from 8.5×10^{-8} (m^3/kg) to 6×10^{-8} (m^3/kg). Carbonate values decrease from 3.5% at the contact with Zone IV and remain negligible until an increase to 1% occurs from 215 to 205 cm, before declining again. Organic matter steadily increases to ~0.5% across the zone.

4.6 Zone VI: 195-145 cm

Zone VI contains two layers, a silt with clay clasts, where the clasts become increasingly abundant upward in the layer. The silt layer comprises 35 cm of the zone and a clay lens that is 10 cm-thick caps the zone. Less than 0.2% sand is observed in the lower silty layer, and no measureable sand occurs in the clay lens. Silt content steadily decreases from 80% to 69% across the silty layer, while clay increases steadily from 20% to 30%. Within the clay lens, silt decreases to 62% and clay increases to 36%. SD averages 1.5 Φ in this poorly sorted zone. Sediments are finely-skewed across the base of the zone and become near-symmetrical at the top of the clay layer.

X_{hf} is 5.5×10^{-8} (m^3/kg) within the basal 5 cm of the silty layer and increases to an average of 7×10^{-8} (m^3/kg) in the lower silt layer and clay layer. Within the upper silt layer, where clay clasts comprise a higher percentage of the sediment, a slight decline in the X_{hf} occurs with an average of 6×10^{-8} (m^3/kg). Carbonate values maintain background levels throughout the zone. Organic matter, however, shows a continuously increasing trend upwards in the zone with values of 0.2% at the base to 1% at the top of the zone.

4.7 Zone VII: 145-75 cm

Zone VII is marked by a light brown-gray diatomite at the base, overlain by a 10 cm-thick light brown diatomite, a 10 cm diatomaceous clayey silt layer, and a 25 cm-thick clayey silt bed that tops the zone. The base of the light brown diatomite contains a 2% sand interval that declines to an average of ~0.1% throughout the layer and overlying diatomaceous clayey silt layers before spiking again to 2% within the lower clayey silt. Initially, silt content increases in the light brown-gray diatomite as clay decreases, but, throughout the remainder of the zone, silt decreases continuously from 83% to 62% and clay increases from 15-36%.

Zone VII is poorly sorted throughout, but, shows slightly better sorting throughout the diatomaceous layers (SD=1.2 to 1.5 Φ) and becomes increasingly poorly

sorted ($SD= 1.7-1.4 \Phi$) throughout the clayey silt. Grains are finely-skewed in much of the diatomaceous layers and border between near-symmetrical and finely-skewed throughout most of the clayey-silt and light-brown diatomite layers, except from 90 to 85 cm-depth where grains are finely-skewed.

X_{hf} drops to 4×10^{-8} (m^3/kg), from values seen in the underlying zone, at the base of the diatomite in this zone and averages 5.5×10^{-8} (m^3/kg) across the remainder of the diatomite layers. Within the diatomaceous clayey silt X_{hf} decreases to $\sim 7.5 \times 10^{-8}$ (m^3/kg) while the lower clayey silt averages 5.75×10^{-8} (m^3/kg), but increases to 8.0×10^{-8} (m^3/kg) in the upper clayey silt layer. Carbonate values maintain background levels of $\sim 0.2\%$ throughout the zone. Shifts in organic matter, however, are discernable. These shifts include an increase to $\sim 0.6\%$ from the base of the zone to 100 cm-depth and a decrease in organic matter in the upper 20 cm of the zone, where values range from 1.1% to 0.8%. An anomalous spike of 1.25% is seen at 105 cm, which corresponds to the sand spike seen in the clayey silt.

4.8 Zone VIII: 75-0 cm

The top portion of the section is comprised of organic-rich sediments; however, three variations within the zone can be identified. At the base of the zone to 50 cm-depth is an organic-rich silt layer with relatively constant silt and clay contents that average 64% and 36%, respectively. Overlying this layer is an organic-rich clayey silt from 45-25 cm that contains a lower silt (57.5%) and higher clay (42.5%) content, and has no measureable amount of sand. The upper 20 cm of the zone is comprised of an organic-rich silt which exhibits a slight increase in silt (60-65%) and sand content ($\sim 0.1\%$), with a decrease in clay values from 39% to 36%, upwards. At 10 cm-depth, the interval contains 2% sand, highest in the zone, as well as the highest silt content (68%) and lowest amount of clay (30%).

Sediments in Zone VIII are poorly sorted throughout, however, the lower organic-rich silt trends toward increasingly poor sorting, whereas the overlying organic-rich clayey silt trends toward better sorting, upward. Sorting remains constant within the upper layer, except for at 10 cm, where sorting is slightly better. Within this zone, all units are near-symmetrical. Skewness within the lower silty layer remains constant, as does the clayey-silt, however, this layer borders on coarsely-skewed. In the upper silt, however, a trend toward finely-skewed exists.

Relatively stable X_{hf} values of $\sim 7.5 \times 10^{-8}$ (m^3/kg) are seen throughout Zone VIII, except for a decrease to 6×10^{-8} (m^3/kg) at 10 cm-depth. Carbonate remains at background levels (0.1%) and organic matter increases continuously from 1% to 1.5% towards the top of the zone. Organic matter spikes at 10 cm to over 2.5%, the highest value seen at the MabX location.

4.9 Metals

The presence of the eight zones is supported by the early transition metals Al, V, Cr, Mn, and Fe (Fig. 4). In zone I, Al, V, Cr, Mn, and Fe metal concentrations vary below 525 cm but, these metals show decreasing concentrations from 525 cm to the top of the zone. In the lower portion of Zone II Al, V, Cr, and Fe decrease overall before

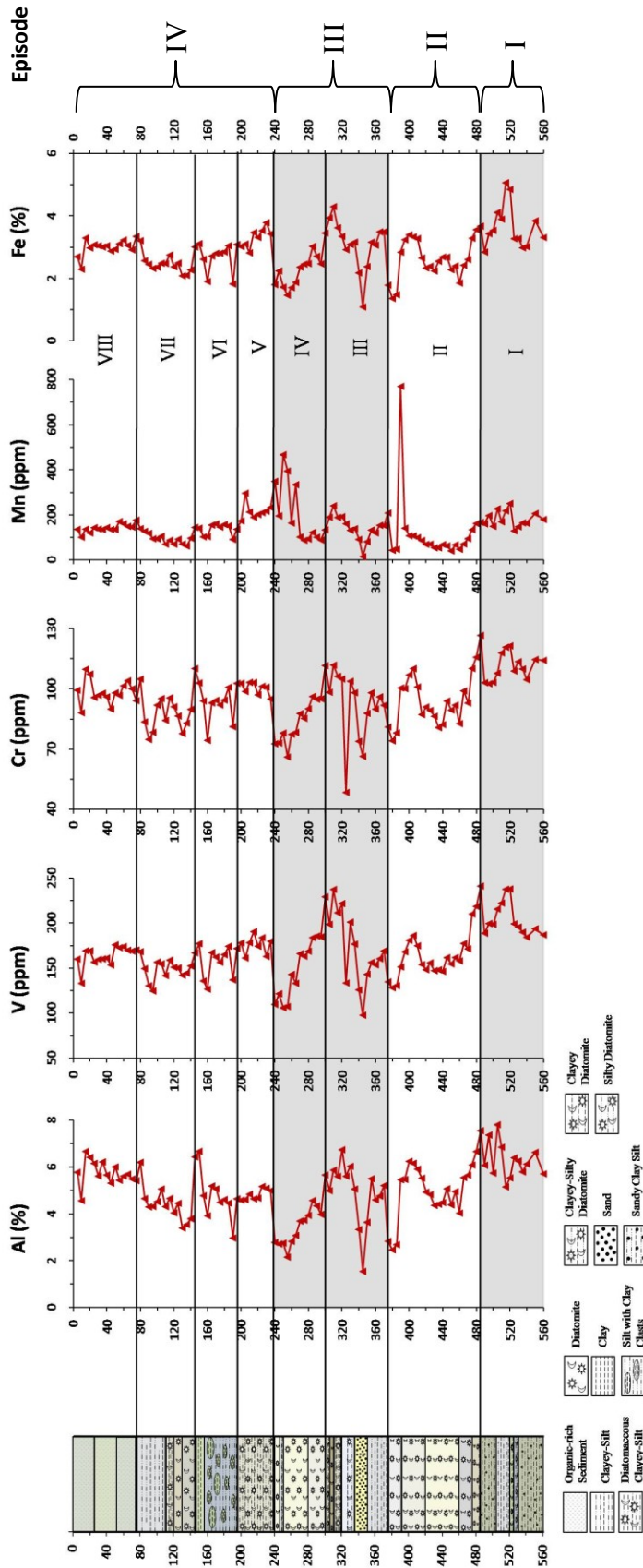


Figure 4: Graphs of transition metal concentrations for Aluminum, Vanadium, Chromium, Manganese, and Iron concentrations compared to the lithologic section. Al and Fe are reported in weight percent (%), all others reported in ppm.

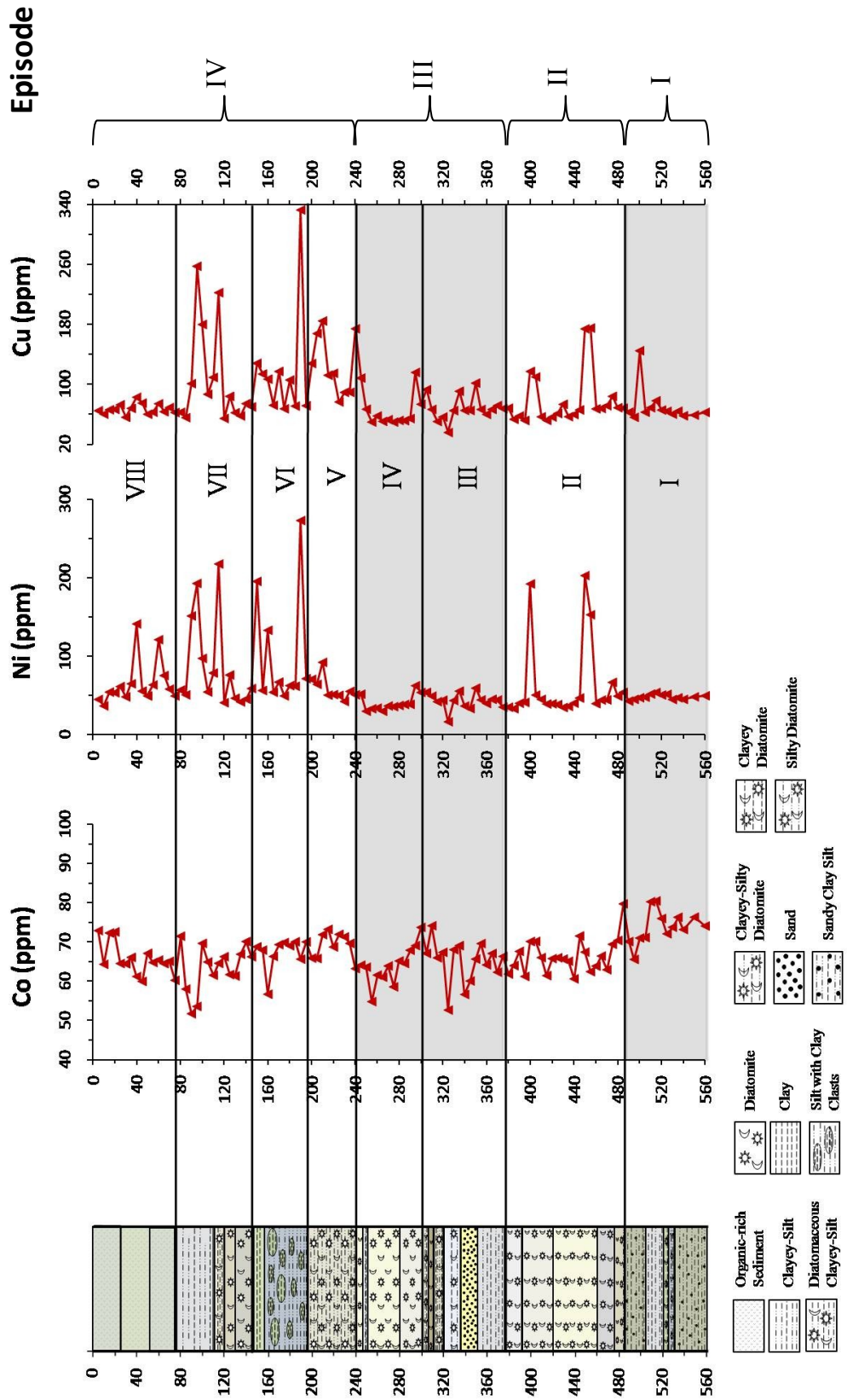


Figure 5: Graph of heavy transition metals Cobalt, Nickel, and Copper concentrations reported in ppm and compared to the lithologic section.

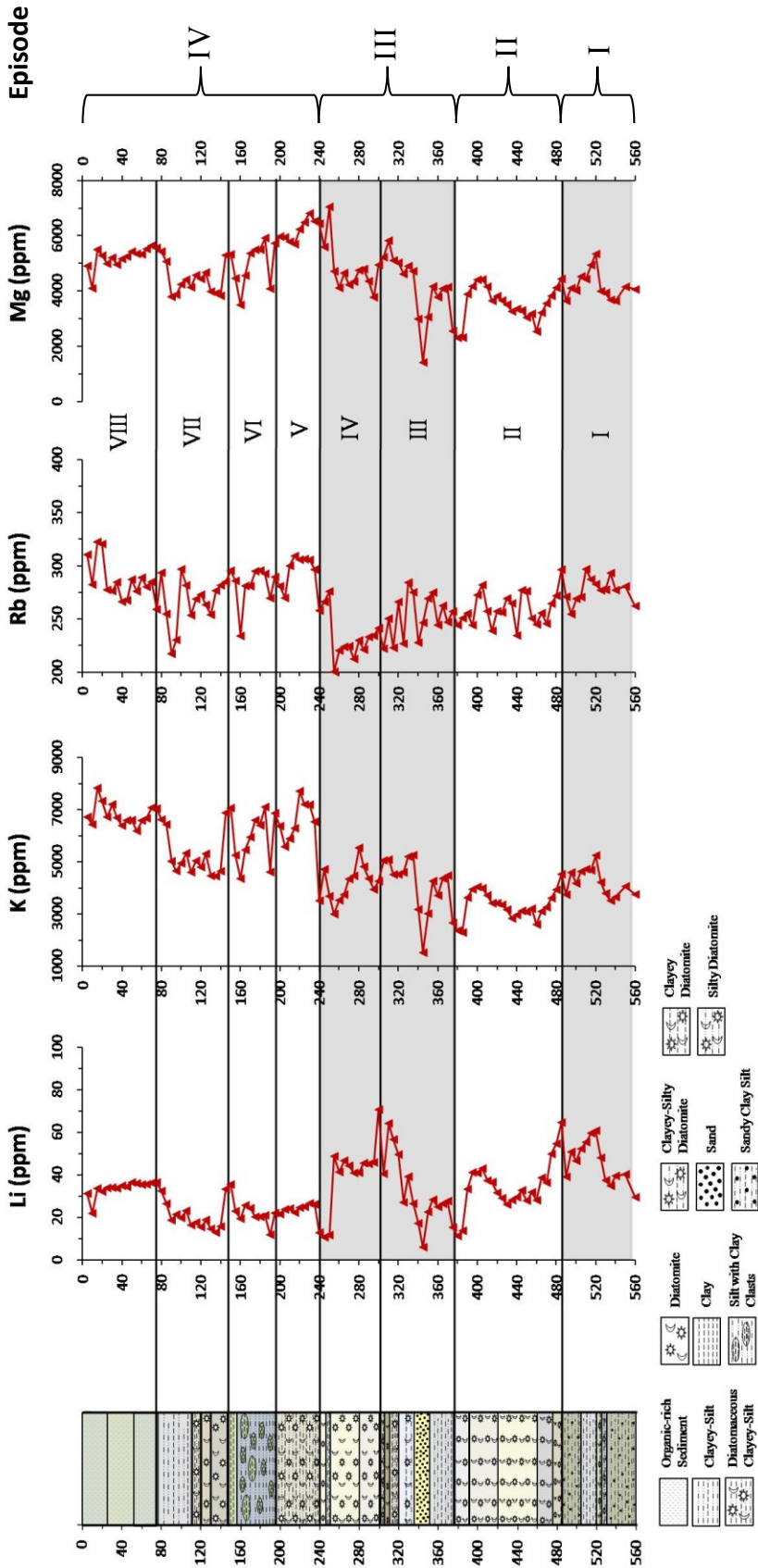


Figure 6: Graphs of Lithium, Potassium, Rubidium, and Magnesium concentrations reported in ppm and compared to the lithologic section.

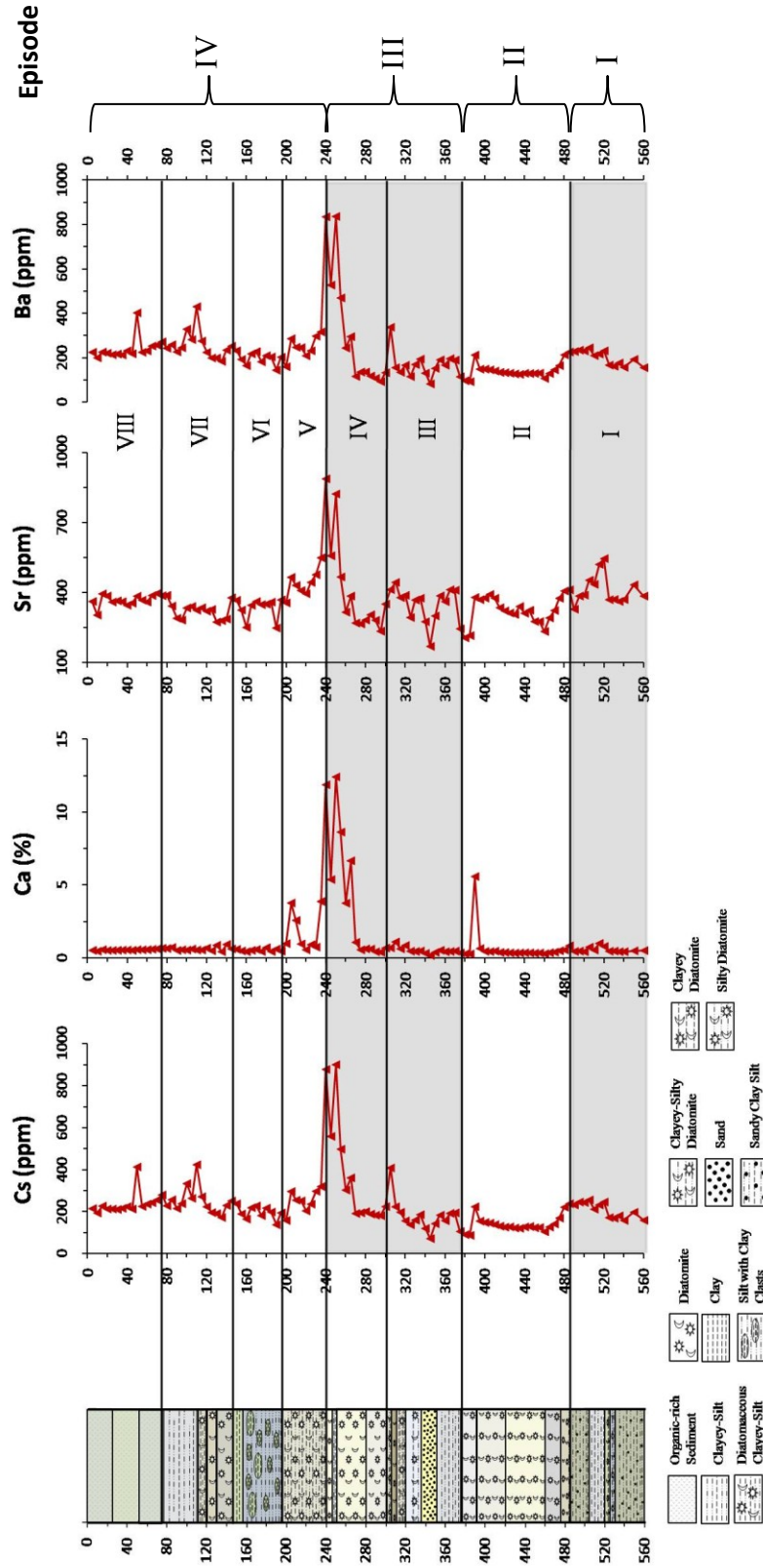


Figure 7: Graphs of concentrations for Cesium, Calcium, Strontium, and Barium. All metals reported in ppm except Ca given in weight percent (%).

increasing with a peak at ~405 cm-depth followed by decreases in the top 15 cm of the zone. Steady increases in Mn concentration, however, occur before a large peak in concentration at 390 cm-depth, which is consistent with an increase in carbonate (Fig. 3). Early transition metals in Figure 6 are relatively constant in the basal 20 cm of Zone III before showing a marked decrease to some of the lowest values in the section within the sand layer. Throughout the remainder of Zone III, these metals increase in concentration, except for a marked decrease in V and Cr observed at 325 cm-depth. Al, V, Cr, and Fe gradually decrease across the Zone IV diatomite layers, while Mn increases in this zone.

Above 240 cm-depth, Al, V, Cr, and Fe show more subtle changes in concentration than below 240 cm and, these metals systematically shift toward higher average concentrations above 240 cm. In Zone V, Al, V, and Cr concentrations tend to fluctuate around average concentrations, while a decrease in Fe and an increase in Mn occur at 205 cm-depth. A concentration spike in Mn at 205 cm-depth is consistent with the occurrence of carbonate (Fig. 3). In Zone VI, the early transition metals decrease at 195 cm-depth and subsequently increase to average values before decreasing again at 160 cm-depth. Above 160 cm-depth, these metals increase in concentration throughout the remainder of the zone. Al, V, Cr, Mn, and Fe concentrations increase overall throughout Zone VII while, Al, V, and Cr decrease from 100 cm to 85 cm-depth. Within Zone VIII, Al increases overall and Mn maintains nearly constant values. Shifts in the concentration of V and Cr, however, occur in Zone VIII that coincide with the organic-rich sediment layers (Fig. 3). A decrease in all early transition metals is observed at 10 cm-depth.

Transition metals Co, Ni, and Cu (Fig. 5) define a unique boundary at 240 cm-depth where concentrations of each metal shifts to higher values above 240 cm than those observed below 240 cm. This boundary event is also present in Li, K, Rb, and Mg concentrations (Fig. 6). Above 240 cm Li concentrations decrease to averages that are among the lowest in the section. Concentrations of K above show an overall increasing trend throughout the section but, shift toward even higher concentrations above 240 cm-depth. Decreasing trends in Rb concentration occur from 560 cm to 240 cm-depth before shifting to higher concentrations above 240 cm-depth. Below 240 cm, Mg concentrations increase but, above 240 cm-depth, Mg has a decreasing trend. Consistent with the the boundary event at 240 cm-depth observed in other metal data sets, Cs, Ca, Sr, and Ba concentrations (Fig. 7) increase considerably from 265 cm to 240 cm-depth, but remain relatively constant throughout the rest of the section.

CHAPTER V

DISCUSSION

Multi-proxy data sets collected in this study can be used to determine the effects of local and regional climatic influence, as well as provide insight as to how the effects of faulting associated with the ORZ can be observed in the lake sediment record. Grain size analysis of sediments within the lake basin is the primary tool used to delineate whether or not sediments being deposited are of local or distal origin. Local sediments supplied by channels such as the Ngwezumba and Gautumbi Rivers (Fig. 1b), as well as from nearby dune fields and beach ridges, for instance, will have a larger average grain size and higher sand content than sediments originating from distal sources such as the Angolan highlands. Allocthonous sediments from Angolan highlands are altered by the fractionating effects of the Okavango Delta swamp and, therefore, will contain higher percentages of silt and clay-sized material, and little, if any, sand-sized sediment by the time the sediments reach Mababe. Additionally, the lithology of the sediment section and the thickness of each of the lithologies can be used to distinguish periods dominated by local and regional sedimentation. The influence of a local climate would result in the occurrence of sand-sized sediments and the appearance of lithologies such as sandy-clay silts, whereas the effects of a regional climate would be manifest in the lake record as clay.

5.1 Tectonics and Lake Sedimentation

5.1.1 Evidence of Tectonism

A major change in the trends of the multi-proxy data is observed at 240 cm-depth. Marked differences in the sedimentation patterns above and below 240 cm are reflected in the relative sand, silt, and clay content and distribution (Fig. 2), as well as the magnitude and variations of the magnetic susceptibility values (Fig. 3). Alkali metals (Li, K, Rb, Be, and Mg) also show major shifts in concentration and distribution patterns above and below 240 cm (Fig. 6). Between 240 and 260 cm, the boundary is characterized by anomalously high carbonate content (Fig. 3) and high concentrations of Cs, Ca, Sr, and Ba (Fig. 7). These changes in the sedimentological and geochemical properties above and below 240 cm reflect variations in allocthonous sediment sources and their relative contribution to the lake sedimentary budget. Allocthonous sediments from local sources supplied to the depression are transported by ephemeral rivers with watersheds in the Kalahari basin (e.g., Burrough and Thomas, 2008). Additionally,

sediments can be brought into the depression from the Angolan highlands via the present day Okavango River, and in the past by the Kwando and Zambezi Rivers (e.g., Shaw, 1985; McCarthy and Metcalfe, 1990; Burrough and Thomas, 2008).

There are fundamental differences in the sediment characteristics and geochemistry of sediments derived locally within the Kalahari basin and those from the upper watershed of the Okavango, Kwando, and Zambezi Rivers. Local sediments from the Kalahari basin consist mainly of aeolian quartz sands and soils rich in calcrete and silcrete (Shaw et al., 2003; Ringrose et al., 2005). Mean grain size of dunefield sediments in the Kalahari range from 2.2 Φ to 3.0 Φ (Cooke, 1980), while the beach ridges around the Mababe Depression range from 0.28 mm to 0.18 mm (1.84 Φ to 2.47 Φ) (Burrough and Thomas, 2008) and averaged 2.6 Φ where sampled along the Magikwe Ridge (Cooke, 1980). Typically the beach ridges near Mababe consist of greater than 90% sand, with silt and clays making up the difference (Burrough and Thomas, 2008; Burrough and Thomas, 2009). Silcretes and calcretes, however, can form as a result of pedogenic and non-pedogenic processes occurring from the semi arid climate of Kalahari basin (McCarthy and Metcalfe, 1990; Nash et al., 1994; Nash and McLaren, 2003; Ringrose et al., 2005).

Sediments derived from the upper watershed of the Okavango, Kwando and Zambezi Rivers are produced by the weathering of bedrock in a tropical climate. These sediment properties can be further modified by processes occurring in swamps before reaching the Mababe Depression. Modern sediments transported by the Okavango River at Mohembo, located at the tip of the Panhandle represent sediments that have not been significantly altered by transport through the swamps of the Okavango Delta. Sediments arriving at Mohembo can therefore be used to infer the characteristics and geochemistry of sediments derived from the upper watersheds of the Okavango and Kwando Rivers in the Angolan highlands.

Extensive swamps of the Okavango Delta can modify sediment distribution by causing preferential loss of the sand-sized fraction as water velocity decreases (McCarthy and Metcalfe, 1990). Sediment size distributions measured near the Panhandle are markedly different than those observed more distally in the delta. Grain size near Mohembo, for example, ranges from 0.2 mm to 0.4 mm (2.3 Φ to 1.3 Φ) (McCarthy et al., 1991). Sediments located near in the permanent swamp area along the Khiandiandavhu channel, however, averaged \sim 0.19 mm (2.4 Φ) (McCarthy and Metcalfe, 1990). Approximately 90% of the sand-sized material is deposited when entering the panhandle region of the Delta (McCarthy and Metcalfe, 1990). Thus, given the modifying effect of the Okavango Delta swamps on sediments transported beyond Mohembo, it can be inferred that the presence of the Linyanti Swamp along the Kwando River, near Mababe, will impact sedimentation in a similar manner by varying the physical and geochemical characteristics of sediments transported from the Angolan highlands.

Sediment grain size distributions indicate that deposition of sand below 240 cm-depth is prominent in the sedimentary record and accounts for up to \sim 10% of the sediments deposited in various layers below 480 cm-depth (Fig. 2). A significant layer of \sim 45% sand occurs at 345 cm-depth with an average grain size of 0.062 mm for the layer. Overall, sediments located at and below 240 cm-depth have an average grain size of 0.017 mm (6.4 Φ). Occurrences of sand above 240 cm are not as significant and average

only ~2% of sediments where sand accumulations are observed (Fig. 2). Sediments above the 240 cm boundary have an average grain size of only 0.01 mm (7.07 Φ) and show a shift towards a finer grain size overall. This suggests that during the time interval above 240 cm, sedimentation was likely dominated by fine-grained allochthonous sediments from the Angolan highlands, compared to locally derived coarser sands. Alternatively, the influx of local sediments into the depression could have declined due to decreased fluvial transport resulting from a locally drier climate.

Differences in the sediment type and geochemistry above and below 240 cm, such as the increased abundance of sediments from the Angolan highlands above 240 cm-depth, suggests a fundamental shift in the source and supply of sediment. An increase in the relative volume of water and sediment load from the Angolan highlands would cause sediments from the Angolan watershed to dominate the lake record at Mababe. Such a shift in the relative proportion of sediments derived from local versus distal sources above and below 240 cm would require a major reorganization of the hydrology of northwestern Botswana.

Reorganization of the hydrology is hypothesized to have changed the proportion of water and sediments from a local source to a system that was dominated by water and sediments transported from the Angolan highlands. Hydrologic reorganization is also hypothesized to affect the residence time of water in the depression. For example, if water were to pool in the Mababe Depression for long periods of time, it could explain the gradual changes in the sedimentary and geochemical characteristics of sediments above 240 cm, such as the steady accumulation of clay-sized material and more systematic shifts in metal concentrations. In comparison, below 240 cm rapid changes occurred during the deposition of sand-sized sediments. Changes observed in the sediment properties above and below 240 cm require that rivers that supplied water and sediments to the Mababe Depression undergo a fundamental change in hydrology, a shift that is attributed to tectonic processes (Huntsman-Mapila et al., 2005).

5.1.2 Tectonic Alteration of Hydrology and Sedimentation

Tectonic processes in the ORZ have caused the geomorphologic form of the delta and the surrounding region to evolve over time, which altered the regional hydrologic system. Presently, topographic evidence suggests two main inlets for rivers flowing from the Angolan highlands into the Mababe depression (Fig. 1b). In the northwest, the Savuti River transports water from the Kwando River through the Savuti swamps and the Tsatsara gap, while in the south, the Mababe River carries water from the Khwai and Thamalakane Rivers, sourced from the Okavango River (Fig. 1b). Given the present day topographic configuration of the Okavango Delta and its' surroundings, lake levels in the Mababe Depression would be controlled by the elevation of the inlets in the northwest and southern portions of the depression.

Lake levels in the Mababe Depression that result from inflow along the Mababe River, at the southern end of the basin, would be controlled by the elevation of the Savuti inlets (~927 m), since lake levels exceeding this elevation would drain through the Savuti channel in the northwest (Fig. 1b). Also, lake levels are controlled by topographic thresholds along the Thamalakane River at 936 m and at 940 m in the channel of the Boteti River that flows into the Makgadikgadi Pans (Gumbrecht et al., 2001). Because of

these topographic thresholds, lake levels rising above 936 m would flood most of the lower delta and inundate Lake Ngami and the Mababe Depression along the Thamalakane axis, resulting in the formation of Paleolake Thamalakane (Shaw, 1988). Post-tectonic topographic controls influence how water and sediment reach the Mababe Depression.

5.1.2.1 Sedimentation Pre-240 cm-depth

Sedimentation below 240 cm requires a different tectonic configuration and hydrologic regime from that above 240 cm. In order for local sediments to dominate sedimentation below 240 cm, lower volumes of river water supplied from the Angolan highlands are required. In the absence of the present day topographic configuration and control on sedimentation in the depression, sedimentation patterns suggest that higher frequency lake level fluctuations occurred below 240 cm. Accumulation of coarse-grained material below 240 cm, and in particular below 485 cm, could represent the influence of a locally wet climate. Lake levels inferred from sediments between 240 cm and 485 cm-depth were sufficiently deep to support the growth and deposition of diatoms (Fig. 2). Therefore, this time period could be the result of a wet climate in Angola, as well as locally, that would have sustained river flow and maintained a deep lake within the Mababe Depression.

5.1.2.2 Sedimentation Post-240 cm-depth

An important aspect in the history of the Mababe Depression is the tilting of the basin, that likely occurred during the tectonic events that reorganized the hydrology of the region. Tilting of the basin led to its' present-day configuration that has resulted in variations in elevation north to south along the 936 m ridge (Gumbrecht et al., 2001). In the absence of a tilted basin, topographic thresholds controlling lake levels in the Mababe Depression would have been different and would have allowed the lake to retain larger volumes of water before outflow would have occurred. Tectonic and hydrologic changes altered how the Mababe Depression was filled with water and also affected sedimentation patterns above 240 cm. Sedimentation appears to have occurred uninterrupted in the basin (below 240 cm) until faulting diverted the Kwando River away from the depression. Okavango Delta sedimentation beginning ~40 ka (Ringrose et al., 2008), may have led to the development of distributary channels that characterize the modern delta configuration. Development of the Okavango Delta led to new landscape conditions that controlled water and sedimentation in the Mababe Depression.

The sedimentation record from the Mababe Depression suggests a timing for the movement along the Linyanti Fault and is marked by the significant change observed at 240 cm-depth in the multi-proxy data sets. Sedimentation above 240 cm-depth occurred after faulting along the Linyanti diverted river inflow away from the Mababe Depression and the Okavango Delta formed, thereby, creating a new hydrologic regime in the area. Grain size distribution of sediments above 240 cm show predominantly silt and clay-sized fractions (Fig. 2) and have a distinct sediment sorting signature and geochemistry that is consistent with the lithologic and chemical fractionation of sediments by marshes in the Okavango and Linyanti deltas. These characteristics indicate that sediments

dominating deposition above 240 cm were sourced primarily from the Angolan highlands.

5.2 Paleoenvironmental History

Climate change can also affect sediment supply and water levels in the Mababe Depression, and the resulting shifts in sediment properties and geochemistry will be superimposed on the record of tectonic processes. The Okavango Delta and lakes in this region are unique in that they can be affected directly by local climate, as well as indirectly by the climate changes in the Angolan highlands. When the timing of local wet periods coincide with that in the Angolan highlands, it may be difficult to separate these events in the sedimentary record. However, when the local climate is dry and the climate in the Angolan highlands is wet, the dry local climate may be recorded by a decrease in local autochthonous sediments in the sedimentary. Sedimentation in the Mababe Depression and other lakes within the region provide a record of both local and regional climate change (Huntsman-Mapila et al., 2005; Burrough and Thomas, 2008; Burrough et al., 2009).

Four major episodes in the history of sedimentation in Paleolake Mababe, thought to represent different climatic conditions, are defined based on grain size distribution, magnetic susceptibility, and geochemical data. These episodes represent sedimentation in the Mababe Depression when lake levels rose above 923 m, the approximate elevation of the sampling site in this study. The sediment depths that define each episode are shown to the right of Figures 2-7. Episodes I and II, which encompass Zones I and II, respectively, represent sedimentation below 240 cm, before movement along the Linyanti and Thamalakane Faults caused a reconfiguration in the regional hydrology. Episode III, which encompasses Zones III and IV, occurs below 240 cm and encompasses the period in which tectonic activities changed the hydrological system. Episode IV, comprised of Zones V, VI, VII, and VIII, occurs under the new hydrologic and tectonic regime and consists of sedimentation above 240 cm.

5.2.1 Episode I (560-485 cm) >65 ka

Episode I is older than 65 ka and encompasses a period in which local climate and the climate in the Angolan headwaters alternately affected sedimentation within the Mababe Depression. Locally wet climatic events are expressed in the sedimentary record as higher influxes of sand-sized sediments and, overall, higher contributions to sedimentation during this episode (Fig. 2). Prior to tectonic activity, that diverted flow of the Kwando River to the Zambezi River, the entire discharge of the Kwando River likely flowed into the Mababe Depression via the inlet of the now underfit Savuti channel and the Tsatsara gap (Grove, 1969; Shaw, 1985). Sedimentation from the Angolan highlands deposited by the Kwando River, however, was likely characterized by higher silt and clay content consistent with higher magnetic susceptibility values (Fig. 3) than those observed in the sandy intervals derived locally.

Lake levels were probably shallow during this episode, as evidenced by rare accumulations of diatoms. Furthermore, the absence of diatom accumulations may indicate the lack of a stable water body in the lake over long time periods. Alternatively,

lake water chemistry was not conducive for diatom growth. The physical properties of the sediments in conjunction with the evidence that lake levels were stable for relatively short periods of time, may indicate that the climate in the Angolan highlands was relatively dry, but, that periodic wet periods occurred within the local climate throughout this interval. Deposition of sediments during the locally wet climate would have masked a dry climate signal in Angola throughout the episode. Overall, sedimentation during Episode I is consistent with a regionally arid climate (Burrough et al., 2009).

5.2.2 Episode II (485-375 cm) ~65 ka to 41 ka

Episode II ranges from ~65 ka to about 41 ka and is characterized entirely by diatomite layers (Fig. 2). Lake levels were likely sufficiently deep to support diatom growth throughout this time period. Therefore, this interval represents a period in which the climate in the Angolan highlands was wet and able to sustain flow to the Mababe Depression. A distal source of sedimentation for this interval is supported by elevated lake levels over the duration of this event. The predominance of diatomite suggests that lake levels were stable above the 924 m elevation for prolonged periods to promote diatom productivity that ultimately generated an ~1 m-thick layer of diatomite. In order to promote the growth and accumulation of extensive diatomite layers, water supplied to the basin must have been high in nutrients and high productivity resulted in excellent preservation of diatoms.

Sediments in this episode as a whole are moderately sorted and very-finely skewed, which are inferred to be characteristics of unfractionated sediments from the Angolan highlands. This is in addition to an overall increase in silt content, indicative of a distal sediment source. A wet climate in the Kwando River headwaters in the Angolan highlands would have been required to sustain lake levels over this ~24,000 year time period. Modeling based on present day evaporation and river discharge rates suggest that the Kwando/Chobe River is capable of providing enough water to maintain a lake of ~2,000 km² in size, which is sufficient to sustain lacustrine conditions in the Mababe depression (Grove, 1969 and references therein). Therefore, in order for the Kwando River to have been the source of sustained water during this time, this episode must have occurred prior to tectonic events that diverted the Kwando River away from the Mababe Depression along the Linyanti Fault.

Although precipitation from a locally wet climate could contribute to the higher lake levels, it is not obvious from the sedimentary evidence in that such a situation occurred for the entire episode. The absence of a predominance of sand that would characterize a local sediment supply can be explained, however, if sand transport to the lake occurred when lake levels were high and the sand was deposited at the mouths of the rivers to form deltas. It is likely then that any sand expected to accompany locally wet climatic conditions was deposited in deltas at the mouths of the Ngwezumba and Gautumbi Rivers (Burrough and Thomas, 2008).

Local climate likely influenced sedimentation during the top 15 cm of Episode II where a significant shift in sedimentation patterns, such as the increase in silt and decrease in clay (Fig. 2) that occur, in conjunction with a decrease in magnetic susceptibility values (Fig. 3). Despite the fact that this interval has the highest silt content in this episode, there is no significant increase in sand (< 1%). Sediments

supplied to the depression that have a low magnetic susceptibility and a decreased abundance of transition metals (Figs. 3 and 4) are interpreted to represent sediments brought in from the local environment and, thus, suggest a wet local climate for this event. Prior to this locally wet climate, a period of drought likely occurred that resulted in evaporation of the lake, increased salinity, and led to the precipitation of carbonate just below the upper diatomite layer (Fig. 3). Carbonate in this interval is likely due to intra-lake processes because concentrations of Ca increased and concentrations of Cs, Sr and Ba that should accompany pedogenic carbonate formation are low (Fig. 7).

5.2.3 Episode III (375-240 cm) 41 ka to < 27 ka

Episode III occurs between 41 ka and < 27 ka, however, no age constraints for the upper boundary are available. This episode represents a period with high variability in local and regional climate. Lake sedimentation over this interval is characterized by an overall shift towards increasing silt and decreasing clay content, variable sorting, and a shift towards finely-skewed grains (Fig. 2). Sediments at the beginning of this episode indicate a local source from a locally wet climate, which is expressed as an increase in sand content with better sorting and skewness. Continuously increasing silt content, however, reflects greater sediment delivery from the Angolan highlands over time and a continuously increasing lake level can be inferred from the overall increase in silt towards the top of this episode. Diatomite-silt mixed sediments followed by predominantly diatomite layers suggests that lake conditions, which initially fluctuated perhaps due to variability in the local climate, became more stable. Stable water levels occurred in the Mababe Depression over long periods of time in order to accumulate thick layers of diatomaceous material.

This episode is marked by a prominent occurrence of carbonate at its terminus (Fig. 3), which can be correlated with a carbonate layer in Lake Ngami (Huntsman-Mapila et al., 2005). Occurrence of the carbonate layer in both lakes, separated by ~275 km, indicates an event of regional magnitude. The carbonate layer in Lake Ngami is dated at ~40 ka, a period when the region was covered by an extensive body of water referred to as Lake Makgadikgadi (Grove, 1969), which had an elevation of 945 m at its highest level and occupied an area of ~60,000 km² (Cooke, 1980) to 80,000 km² (Mallick et al., 1981). Lake Makgadikgadi encompassed an area that included the current Makgadikgadi pans, a large portion of the current delta, Lake Ngami, the Mababe Depression and, extends into the Chobe-Zambezi River Valley and Caprivi Strip in the Zambezi area (Grove, 1969; Shaw and Thomas, 1988), although the Zambezi area is not considered in the size estimates (Thomas and Shaw, 1991).

The origin of these extensive carbonates throughout the lakes during this episode is not clear. Two possible sources of the carbonate include the erosion of local calcretes, or, authigenic precipitation within the lake itself. It is hypothesized that the carbonates are local in origin and were derived from erosion of local calcretes. Formed during a previously dry period, these calcretes could have been eroded by local rains and deposited within the lake basins. This is consistent with a locally wet climate that contributed to the formation of Lake Makgadikgadi (Cooke and Verhagen, 1977; Shaw and Cooke, 1986). However, there is also a lack of local sands during this time that would have been an integral part of the sediment record, and is inconsistent with the

hypothesis of extensive erosion required to deposit the calcretes. Alternatively, formation of the carbonates within the lake would require evaporation to achieve carbonate saturation, as observed in other lakes of the Kalahari region during dry periods (Thomas et al., 2003). In such a scenario, there should be a regionally equivalent carbonate layer present in soils in non-lake basins that should correlate with those observed in Lake Ngami (Huntsman-Mapila et al., 2005) and the Mababe Depression. Because of the paucity of sedimentary geochemical data, further research is needed to verify or refute calcrete erosion or *in-situ* precipitation as the source of the carbonates.

Lake Makgadikgadi at a 945 m elevation would not have been constrained by topography given that it is believed to have been both a locally and regionally wet climate. Constraints to the lake level would have been a mechanism for draining such an extensive lake. An outlet hypothesized to have drained the lake was through tectonic controls to the north of the Mababe Depression, which likely would have drained the lake into the Zambezi River via the Kwando/Chobe River (Grey and Cooke, 1977). Alternatively, the waters of the lake could have evaporated over time.

5.2.4 Episode IV (240-0 cm) < 41 ka

Episode IV has no age-constraint at its' lower boundary, but was dated at 135 cm-depth at 27 ka. This episode is controlled primarily by climate variations in the Angolan highlands and is represented by sediments from 240 cm-depth to the surface. The sediments above 240 cm-depth are attributed to the Lake Makgadikgadi stage and suggest a different hydrologic regime could have been initiated by local or regional tectonics. Reactivation of the rift faults would have altered the region in two main ways: 1) cutoff of the Kwando River as a regular source filling the Mababe depression by diversion of the Kwando River via faulting to form the Linyanti-Chobe River, which served as a drainage pathway into the Zambezi River and 2) the impoundment of the Okavango River and initiation of the formation and development of the delta to its current form. The end of Episode III was due to a tectonic interplay that created a new hydrologic regime in the region and altered sedimentation and geochemistry patterns observed in Mababe depression sediments above 240 cm-depth.

Water brought into the Mababe Depression from the Angolan highlands during this Episode was likely a result of inflow from the Okavango River because tectonic activities had previously diverted the Kwando River, the main source of water to the Mababe Depression, to the Zambezi River. Even though the Okavango River became the new regular source of water to the Mababe depression, after the Kwando River was diverted, a topographic control (knob) at 936 m elevation along the Thamalakane River caused flow into the Mababe depression to occur only during regionally wet and extremely wet local periods. River water flowed into the Mababe Depression via the Khwai River to sustain marsh-like conditions. The elevation to which the lake levels could rise during local wet periods was restricted by the elevation at the inlet of the Savuti channel which can serve as an outlet, except during regional flooding events.

Assuming no erosion of sediments has occurred in the depression, there is no evidence of waning from Lake Makgadikgadi at the 945 m level to completely dry conditions (Fig. 2). Instead, the sediment record shows an abrupt change in sediment characteristics and geochemistry, which remained nearly constant for a prolonged time

(~240 to 195 cm). The lack of a characteristic decrease in clay associated with a desiccation event is not observed in this zone. Grey and Cooke (1977) hypothesized that reactivation of the Linyanti fault, which diverted the Kwando River through the Linyanti-Chobe River to the Zambezi River, could have provided an outlet for draining Lake Makgadikgadi. The sediment record suggests that if Lake Makgadikgadi was being drained in this manner, it would leave evidence in the sediment record of drainage in the form of constant sediment type.

The first occurrence of sediments in this episode are those of Zone V. This period is marked by a relatively stable lake levels sourced from the Angolan highlands, as evidenced by the lack of sand accumulation. Clay and silt levels also remain fairly constant throughout the zone, indicating the source of sediments remained constant. Prior to the end of this zone, a layer containing carbonate of similar nature to that observed in Episode III occurs, but its origin also remains unclear.

Following stable lake conditions, a decline in lake levels is marked by an increase in clay content from ~18% to 38% throughout Zone VI. Organic matter also increases throughout the zone and represents the encroachment of aquatic and wetland vegetation at the sample site as lake levels declined. A brief period of local climate influence occurs at 165 cm-depth, resulting in a small increase in sand content (Fig. 2).

Lake levels rise again between Zone VI and VII. This rise in lake levels is evidenced by the return of diatomite and diatomaceous clayey-silt layers at the base of Zone VII that overlie clay-rich beds in Zone VI. The early part of Zone VII is characterized by a sharp increase in silt and decrease in clay. This is coupled with a decrease in organic matter at the base of the zone that may represent deeper water conditions that do not support aquatic plants at the sample site. Rising lake levels of this interval were likely the result of increased water supply from the Angolan highlands, coupled with an increase of sediments from a wetter local climate, as indicated by higher sand sedimentation that exceeds 2%. An age constraint of ~27 ka is given during this wet interval at 135 cm-depth.

Throughout the remainder of Zone VII lake levels begin to decline but a shallow lake level is maintained by a periodic supply of water into the lake. Overall, clay content increases and silt decreases, although fluctuations occur throughout Zone VII (Fig. 2). While the sediment geochemistry and organic matter content show fluctuations, few changes in metal concentrations occur (Figs. 2, 3, 4, 5, 6, and 7). These fluctuations in the sediment and sediment geochemistry support a shallow lake that periodically receives water. During low lake levels organic matter concentrations increase as marsh-like conditions prompted vegetation growth in the lake basin.

Within the organic-rich sediment layers of Zone VIII one age date of 11.7 ka is available at 45 cm-depth. Marsh-like conditions likely dominated the zone, as evidenced by the higher levels of organic matter. Alternatively, increases in organic matter may be the result of increased inflow from the Okavango River bringing in organic matter. Higher lake levels likely occurred during this zone when shifts occurred in the clay content. At 10 cm-depth, a brief lake highstand occurs that is evidenced by a drop in clay and X_{hf} and an increase in organic matter as more water is brought into the lake. This event is consistent with a wetter local climate, as evidenced by the increase in sand.

When lake levels decline, as in Zone VI and VII, changes in sedimentation and chemical sedimentation patterns can be observed. Figure 8 depicts the desiccation of the

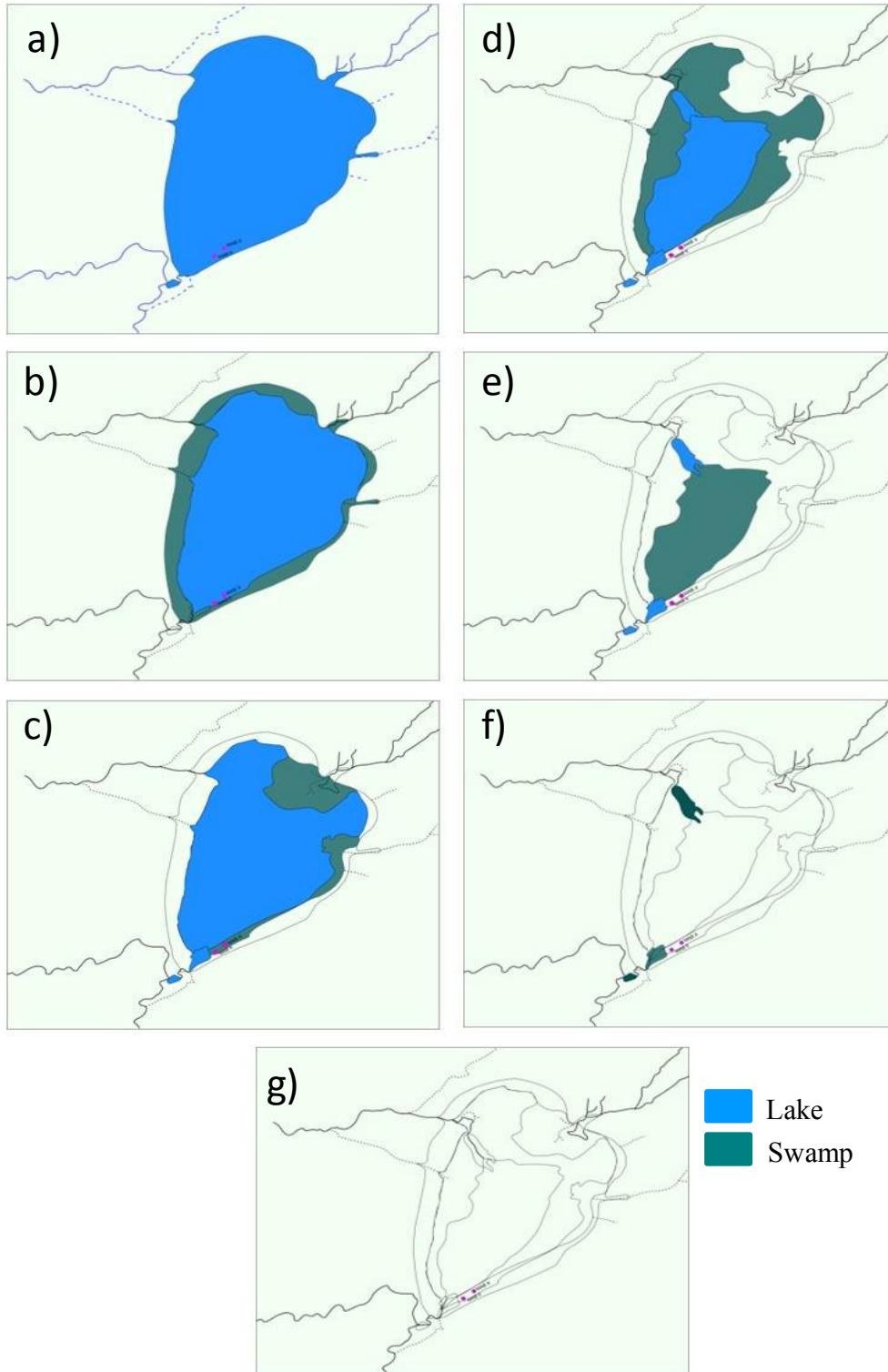


Figure 8: A conceptual model for the draining of Lake Mababe where a) is a full lake b) drying lake with swamp formation c) lake margins are dry and further swamp development d) only the sump and inlets contain water e) the sump has become swampland and only inlets contain water f) inlets are swamps and lake is otherwise dry and, g) total desiccation of Lake Mababe

lake in the Mababe Depression and how changes in lake levels will affect sedimentation at the sample location. As lake levels decline, as in Figure 8b and 8c, vegetation will begin to invade the sample site and promote aquatic and wetland vegetation growth. As marsh conditions move close to the sump, as depicted in Figure 8d and 8e, more terrestrial plant growth will occur at the sample site. Currently the Mababe Depression is represented by Figure 8f, where only the swamps retain water.

5.3 Paleoclimate

Periods of elevated lake levels in the Mababe Depression with available age-constraints can be correlated to lake highstand events in the Makgadikgadi and Ngami basins. A regional paleo-shoreline research program utilizing OSL dating techniques establishes a chronology of lake highstand events over the last 300 ka for Lake Makgadikgadi (Burrough et al., 2009), Lake Ngami (Burrough et al., 2007), and the Mababe Depression (Burrough and Thomas, 2008). The work of Burrough and Thomas (2008) established lake highstand events in the Mababe Depression over the last ~40 ka based on beach ridges, while this study, based on sediment samples, extends the paleo-lake record to > 64 ka. Comparisons made with data from lake highstands is qualitative in nature given that beach ridges preserve only the most recent lake highstands. Additionally, processes responsible for the formation of ridges occur over a much shorter time span compared to the duration of high lake levels.

Based on the limited OSL dates available from this study, the ages of lake highstand events of regional extent (Burrough et al., 2009), and those reported in the Mababe Depression (Burrough and Thomas, 2008) appear to occur in close proximity to the deposition of sediments with high clay content, such as clayey-silt layers and clay layers (Fig. 2). Clay-rich sediments representing high lake levels near the end of Episode I (520-505 cm) were deposited around 64.8 ka. This age is close to that of a lake highstand determined in the Makgadikgadi basin at ~64 ka (Burrough et al., 2009) and Lake Ngami around 59 ka (Burrough and Thomas, 2008). A 20 cm-thick silty-clay layer occurs at the beginning of Episode III (~375 cm depth) that may represent higher lake levels. Sedimentation during this lake highstand occurred ~41 ka, based on an age obtained in the underlying diatomite layer. It is reasonable to suggest that high lake levels that occurred during this interval may correspond to lake highstands determined in the Makgadikgadi basin at 39 ka (Burrough et al., 2009), however, equivalent lake highstands are not reported for Lake Ngami during this period. Hunstman-Mapilla et al. (2005) describe sediments in Lake Ngami ~40 ka, but provide no clear indication if this represented high lake levels that correspond to lake highstands.

During Episode IV, an age of 27 ka was determined from a diatomite layer at 135 cm-depth. This diatomite layer is located above clay-rich layers and suggests that high lake levels occurred prior to 27 ka. This age is also consistent with lake highstands observed in the Makgadikgadi basin ~27 ka (Burrough et al., 2009). This age also post-dates a sharp decrease in clay content between Zones VI and VII that represents an increase in lake levels within the Mababe Depression. Sand accumulations occur above and below the boundary between the declining lake-stage in Zone VI and the high lake levels that mark the onset of Zone VII. These sands are representative of sediments derived during a wet local climate and may correspond to a wet local climate observed in

Drotsky's Cave ~29 ka (Cooke and Verhagen, 1977; Shaw and Cooke, 1986). Although age dates are not available in Zone VI, the interval is believed to represent a lake desiccation event that may correspond to a drier climate associated with periods of dune building documented by O'Connor and Thomas (1999) from 32 ka to 28 ka and by Thomas et al., (2000) from 36 ka to 39 ka. Despite the fact that the lake highstand record for the Mababe Depression extends over 40 ka, beach ridges are not reported by Burrough and Thomas (2008) or in the Makgadikgadi basin by Burrough et al (2009) between 32 ka and 28 ka. Lake highstands were identified in Lake Ngami by Burrough et al. (2007) between 32 ka and 30 ka, however, Huntsman-Mapila et al. (2006) do not provide descriptions that indicate a high lake level for this time period. A clay layer is observed at 245 cm-depth that may also represent high lake levels in the Mababe Depression that occurred between 41 ka and 27 ka and, may be equivalent to lake highstands reported by Burrough et al. (2007) for Lake Ngami about 38 ka.

A clay-rich sediment layer is observed from 100 cm to 75 cm-depth that is younger than 27 ka and older than ~12 ka, an age that was determined at 40 cm-depth. Lake highstands ranging between 17 ka and 12 ka are reported for the Makgadikgadi basin, the Mababe depression, and Lake Ngami (Burrough et al., 2009; Burrough and Thomas, 2008; Burrough et al., 2007). Huntsman-Mapila et al. (2006) describe a locally wet phase that sustained lake levels in Lake Ngami around this period as well. The last clay-rich layer observed in the sediment section occurs from 45 cm to 25 cm-depth and is younger than ~12 ka. Burrough et al. (2009) and Burrough and Thomas (2008) report a lake highstand in Lake Ngami at ~9 ka and Huntsman-Mapila et al. (2006) also report increasing lake levels around 4 ka in Lake Ngami.

Attempts to reconcile high lake levels with lake highstands suggest that although the events could not be directly correlated, the number of occurrences of high lake levels that produced preserved beach ridges appear consistent. It is important to note, however, that if clay layers are a record of high lake levels, not all clay layers will correspond to beach ridges because beach ridges are susceptible to being reworked by subsequent highstands. Processes that produce beach ridges relative to high lake levels operate on different time scales, and, thus, may account for the discrepancies between the ages of the beach ridges compared to recorded ages of the high lake levels.

CHAPTER VI

CONCLUSIONS

Mutli-proxy data collected from the Mababe Depression preserves a record of climate change and tectonic controls that affected the Middle Kalahari environment over the last > 64 ka. A major change in sedimentation occurs at 240 cm-depth at the sample site that records a different series of climatic and tectonic controls affecting sedimentation above and below this boundary. Events that can be discerned in the sedimentary record of Lake Mababe include:

- 1) Sedimentation influenced mainly by the local climate during a period of relatively dry conditions in the catchment area of Angola occurred from 560-485 cm-depth, until ~64 ka.
- 2) This episode was followed by relatively stable lacustrine conditions until ~41 ka. Lake levels were maintained largely by the influx of water and sediment from the Kwando River during a wet climatic period in Angola. Local climatic influence was minimal during this period, as evidence by the low levels of sand accumulation throughout the interval.
- 3) Following the stable lacustrine conditions, lake levels were affected by the input of multiple sources from the local and regional environment. This time period corresponds to the Lake Makgadikgadi stage identified in the area. During this same interval, from 375-240 cm, tectonic movement diverted the Kwando River away from the Mababe Depression and the present-day Okavango Delta began forming. These events permanently altered the hydrologic regime of the area and affected how sediments and water were transported to Lake Mababe.
- 4) Sedimentation above 240 cm reflects a post-tectonic period and the onset of new hydrologic controls and sedimentation patterns within the depression. Without a sustained river source flowing into Lake Mababe, river levels were controlled primarily by input from the Okavango River during wet climatic periods in Angola. The highest lake levels observed during this interval may reflect events that correspond to Lake Thamalakane stages observed elsewhere in the region.

CHAPTER VII

FUTURE WORK

Although this study has enhanced the existing record for paleo-lake Mababe, and, in doing so, has provided additional information on the climate and tectonic setting of the region over the last >64 ka, further research needs to be conducted. Studies focused on understanding the species of diatoms found in the lake record, as well as the paleosalinity of the lake could only enhance the current understanding of paleo-lake levels. These types of studies may provide a more-detailed understanding of lake fluctuations as they relate to the paleo-climate of the region, and may also indicate whether changes in lake levels were basin specific. Additional studies on sediments from within the lake that include stable isotope data, C:N ratios, and nutrient status may confirm whether declining lake levels discussed in this work in fact resulted in an observable shift in the type of vegetation at the sample location and paleoproductivity indicated by diatoms.

Sediments also need to be collected from elsewhere in the basin, such as near the Savuti and Ngwezumba inlets, as well as within the sump, in order to provide additional locations for correlation of lake events. These locations will provide a clearer understanding of the history of Lake Mababe. Additional locations would also indicate whether or not the sample location creates a bias in the sediments and, therefore, the interpretation of lake levels and the paleoclimate of the region. A sample interval of 5 cm, and not to exceed 10 cm, is recommended in similar studies within the Mababe Depression because a larger sample interval will by-pass rapid changes known to occur within the lake and would make correlations increasingly difficult.

In an effort to extricate the source of sediments being supplied to the Mababe Depression, it is imperative that samples be collected from the Okavango, Kwando, and Zambezi Rivers. Analyzing the grain size, particularly in the Kwando and Zambezi Rivers where this information is lacking, as well as metal concentration and water chemistry of sediments supplied by these rivers may indicate unique markers that can identify sediments being supplied to the Mababe Depression from individual rivers.

REFERENCES

- Adamiec, G. and Aitken, M.J., 1998, Dose-rate conversion factors: update: *Ancient TL*, v. 16, p. 37-50.
- Barbouti, A. and Rastin, B., 1983, A Study of the Absolute Intensity of Muons at Sea Level and under Various Thicknesses of Absorber: *Journal of Physics G-Nuclear and Particle Physics*, v. 9, 1577-1595.
- Brook, G.A., Marais, E., Srivastava, P., Jordan, T., 2007, Timing of lake-level changes in Etosha Pan, Namibia, since the middle Holocene from OSL ages of relict shorelines in the Okondeka region: *Quaternary International*, v. 175, p. 29–40.
- Burrough, S.L., and Thomas, D.S.G., 2008, Late Quaternary lake-level fluctuations in the Mababe Depression: Middle Kalahari palaeolakes and the role of Zambezi inflows: *Quaternary Research*, v. 69, p. 388-403.
- Burrough, S.L., and Thomas, D.S.G., 2009, Geomorphological contributions to palaeolimnology on the African continent: *Geomorphology*, v. 103, p. 285-298.
- Burrough, S.L., Thomas, D.S.G., Shaw, P.A., and Bailey, R.M., 2007, Multiphase quaternary highstands at lake Ngami, Kalahari, northern Botswana: *Palaeogeography Palaeoclimatology Palaeoecology*, v. 253, p. 280-299.
- Burrough, S.L., Thomas, D.S.G., Bailey, R.M., 2009, Mega-Lake in the Kalahari: A Late Pleistocene record of the Palaeolake Makgadikgadi system, *Quaternary Science Reviews*, v. 28, p. 1392-1411.
- Cooke, H.J., 1975, Paleoclimatic Significance of Caves and Adjacent Landforms in Western Ngamiland, Botswana: *Geographical Journal*, v. 141, p. 430-444.
- Cooke, H.J., 1980, Landform Evolution in the Context of Climatic-Change and Neo-Tectonism in the Middle Kalahari of North-Central Botswana: *Transactions of the Institute of British Geographers*, v. 5, p. 80-99.
- Cooke, H.J., Verhagen, B.Th., 1977, The dating of cave development—an example from Botswana, *in Proceedings of the Seventh International Speleological Congress*, Sheffield, UK, p. 122–124.

- Cooke, H.J., and Verstappen, H.T., 1984, The Landforms of the Western Makgadikgadi Basin in Northern Botswana, with a Consideration of the Chronology of the Evolution of Lake Palaeo-Makgadikgadi: *Zeitschrift Fur Geomorphologie*, v. 28, p. 1-19.
- Dinçer, T., Hutton, L.G. and Kuppe, B.B.J., 1979, Study, using stable isotopes, of flow distribution, surface-groundwater relations and evapotranspiration in the Okavango Swamp, Botswana: Vienna, In: *Isotope Hydrology 1978*, Vol. I. IAEA, p. 3-26.
- Ellwood, B.B., Harrold, F.B., Benoist, S.L., Thacker, P., Otte, M., Bonjean, D., Long, G.J., Shahin, A.M., Hermann, R.P., and Grandjean, F., 2004, Magnetic susceptibility applied as an age-depth-climate relative dating technique using sediments from Scladina Cave, a Late Pleistocene cave site in Belgium: *Journal of Archaeological Science*, v. 31, p. 283-293.
- Ellwood, B.B., Tomkin, J.H., Ratcliffe, K.T., Wright, M., and Kafafy, A.M., 2008, High-resolution magnetic susceptibility and geochemistry for the Cenomanian/Turonian boundary GSSP with correlation to time equivalent core: *Palaeogeography Palaeoclimatology Palaeoecology*, v. 261, p. 105-+.
- Fairhead, J.D., and Girdler, R.W., 1969, How Far Does Rift System Extend through Africa: *Nature*, v. 221, p. 1018-1020.
- Folk, R.L., and Ward, W.C., 1957, Brazos River Bar: A Study in the Significance of Grain Size Parameters: *Journal of Sedimentary Petrology*, v. 27, p. 3-26.
- Grey, D.R.C., and Cooke, H.J., 1977, Some problems in the quaternary evolution of the landforms in northern Botswana: *Catena*, v. 4, p. 123-133.
- Grove, A.T., 1969, Landforms and Climatic Change in Kalahari and Ngamiland: *Geographical Journal*, v. 135, p. 191-212.
- Gumbrecht, T., McCarthy, T.S., and Merry, C.L., 2001, The topography of the Okavango Delta, Botswana, and its tectonic and sedimentological implications: *South African Journal of Geology*, v. 104, p. 243-264.
- Huntsman-Mapila, P., Kampunzu, A.B., Vink, B., and Ringrose, S., 2005, Cryptic indicators of provenance from the geochemistry of the Okavango Delta sediments, Botswana: *Sedimentary Geology*, v. 174, p. 123-148.
- Huntsman-Mapila, P., Ringrose, S., Mackay, A.W., Downey, W.S., Modisi, M., Coetzee, S.H., Tiercelin, J.J., Kampunzu, A.B., and Vanderpost, C., 2006, Use of the geochemical and biological sedimentary record in establishing palaeoenvironments and climate change in the Lake Ngami basin, NW Botswana: *Quaternary International*, v. 148, p. 51-64.

- Kampunzu, A.B., Bonhomme, M.G., and Kanika, M., 1998, Geochronology of volcanic rocks and evolution of the Cenozoic Western Branch of the East African Rift System: *Journal of African Earth Sciences*, v. 26, p. 441-461.
- Kinabo, B.D., Atekwana, E.A., Hogan, J.P., Modisi, M.P., Wheaton, D.D., and Kampunzu, A.B., 2007, Early structural development of the Okavango rift zone, NW Botswana: *Journal of African Earth Sciences*, v. 48, p. 125-136.
- Kittrick, J. A., and Hope, E. W., 1963, A Procedure for the Particle-Size Separation of Soils for X-Ray Diffraction Analysis: *Soil Science*, v. 96, p. 319-325.
- Mallick, D.I.J., Habgood, F., Skinner, A.C., 1981, A geological interpretation of Landsat imagery and air photography of Botswana: *Overseas Geological Mineral Research*, v. 56, p. 1-36.
- McCarthy, T.S., and Ellery, W.N., 1998, The Okavango Delta: *Transactions of the Royal Society of South Africa*, v. 53, p. 157-182.
- McCarthy, T.S., and Metcalfe, J., 1990, Chemical Sedimentation in the Semiarid Environment of the Okavango Delta, Botswana: *Chemical Geology*, v. 89, p. 157-178.
- McCarthy, T.S., McIver, J.R., Cairncross, B., 1986, Carbonate accumulation on islands in the Okavango Delta, Botswana: *South African Journal of Science*, v. 82, p. 588-591.
- McCarthy, T.S., McIver, J.R., and Verhagen, B.Th., 1991, Groundwater evolution, chemical sedimentation and carbonate brine formation on an island in the Okavango Delta swamp, Botswana: *Applied Geochemistry*, v. 6, p. 577-595.
- McCarthy, T.S., Bloem, A., Larkin, P.A., 1998. Observations on the hydrology and geohydrology of the Okavango Delta. *South African Journal of Geology* 101, 101-117.
- McCarthy, T. S., Smith, N. D.; Ellery, W. N.; Gumbrecht, T., 2002, The Okavango Delta-semiarid alluvial-fan sedimentation related to incipient rifting, *in* Renault, R.W., and Ashley, G.M., eds., *Sedimentation in continental rifts: Special Publication - Society for Sedimentary Geology (SEPM)*, v. 73, p. 179-193.
- Modisi, M.P., 2000, Fault system at the southeastern boundary of the Okavango Rift, Botswana: *Journal of African Earth Sciences*, v. 30, p. 569-578.
- Modisi, M.P., Atekwana, A.E., Kampunzu, A.B., Ngwisanyi, T.H., 2000, Rift kinematics during the incipient stages of continental extension: Evidence from the nascent Okavango Rift basin, NW Botswana: *Geology*, v. 28, p. 939-942.

- Nash, D.J., and McLaren, S.J., 2003, Kalahari valley calcretes: their nature, origins, and environmental significance: *Quaternary International*, v. 111, p. 3-22.
- Nash, D.J., Thomas, D.S.G., and Shaw, P.A., 1994, Siliceous duricrusts as palaeoclimatic indicators: evidence from the Kalahari desert of Botswana: *Palaeogeography Palaeoclimatology Palaeoecology*, v. 112, p. 279-295.
- O'Connor, P.W., and Thomas, D.S.G., 1999, The Timing and Environmental Significance of Late Quaternary Linear Dune Development in Western Zambia: *Quaternary Research*, v. 52, p. 44-55.
- Otvos, E.G., 2000, Beach ridges—definitions and significance: *Geomorphology*, v. 32, p. 83–108.
- Passarge, S., 1904, *Die Kalahari*: Berlin, Dietrich Reimer.
- Prescott, J. R. and L. G. Stephan . 1982, The contribution of cosmic radiation to the environmental dose for thermoluminescence dating: latitude, altitude and depth dependencies: *Journal of the European Study Group on Physical, Chemical and Mathematical Techniques Applied to Archaeology*, v. 6, p. 17–25.
- Ringrose, S., Huntsman-Mapila, P., Kampunzu, A.B., Downey, W., Coetzee, S., Vink, B., Matheson, W., and Vanderpost, C., 2005, Sedimentological and geochemical evidence for palaeo-environmental change in the Makgadikgadi subbasin, in relation to the MOZ rift depression, Botswana: *Palaeogeography Palaeoclimatology Palaeoecology*, v. 217, p. 265-287.
- Ringrose, S., Huntsman-Mapila, P., Downey, W., Downey, W., Coetzee, S., Fey, M., Vanderpost, C., Vink, B., Kemosidile, T., Kolokose, D., 2008, Diagenesis in Okavango fan and adjacent dune deposits with implications for the record of palaeo-environmental change in Makgadikgadi–Okavango–Zambezi basin, northern Botswana: *Geomorphology*, v. 101, p. 544-557.
- Sastre, J., Sahuquillo, A., Vidal, M., and Rauret, G., 2002, Determination of Cd, Cu, Pb and Zn in environmental samples: microwave-assisted total digestion versus aqua regia and nitric acid extraction: *Analytica Chimica Acta*, v. 462, p. 59-72.
- Scholz, C.H., Contreras, J.C., 1998, Mechanics of continental rift architecture: *Geology*, v. 26, p. 967-970.
- Scholz, C.H., Koczynski, T.A., Hutchins, D.G., 1976, Evidence for Incipient Rifting in Southern Africa: *Geophysical Journal of the Royal Astronomical Society*, v. 44, p. 135-144.
- Shaw, P., 1985, Late Quaternary Landforms and Environmental-Change in Northwest Botswana - the Evidence of Lake Ngami and the Mababe Depression: *Transactions of the Institute of British Geographers*, v. 10, p. 333-346.

- Shaw, P., 1988, After the Flood - the Fluvio-Lacustrine Landforms of Northern Botswana: *Earth-Science Reviews*, v. 25, p. 449-456.
- Shaw, P.A., and Cooke, H.J., 1986, Geomorphic Evidence for the Late Quaternary Paleoclimates of the Middle Kalahari of Northern Botswana: *Catena*, v. 13, p. 349-359.
- Shaw, P.A., and Thomas, D.S.G., 1988, Lake Caprivi: A late Quaternary link between the Zambezi and middle Kalahair drainage systems: *Zeitschrift Fur Geomorphologie*, v. 32, p. 329-337.
- Shaw, P.A., Cooke, H.J., Thomas, D.S.G., 1988, Recent advances in the study of Quaternary landforms in Botswana: *Palaeoecology of Africa*, v. 19, p. 15–26.
- Shaw, P.A., Bateman, M.D., Thomas, D.S.G., and Davies, F., 2003, Holocene fluctuations of Lake Ngami, Middle Kalahari: chronology and responses to climatic change: *Quaternary International*, v. 111, p. 23-35.
- Sperazza, M., Moore, J.N., and Hendrix, M.S., 2004, High-resolution particle size analysis of naturally occurring very fine-grained sediment through laser diffractometry: *Journal of Sedimentary Research*, v. 74, p. 736-743.
- Stainstreet, I.G., McCarthy, T.S., 1993, The Okavango Fan and the classification of subaerial fan systems: *Sedimentary Geology*, v. 85, p. 115-133.
- Thomas, D.S.G., Shaw, P.A., 1991, *The Kalahari Environment*: Cambridge, Cambridge University Press, p. 284.
- Thomas, D.S.G., Shaw, P.A., 2002, Late Quaternary environmental change in central southern Africa: new data, synthesis, issues and prospects: *Quaternary Science Reviews*, v. 21, p. 783–797.
- Thomas, D.S.G., O'Connor, P.W., Bateman, M.D., Shaw, P.A., Stokes, S., and Nash, D.J., 2000, Dune activity as a record of late Quaternary aridity in the Northern Kalahari: new evidence from northern Namibia interpreted in the context of regional arid and humid chronologies: *Palaeogeography Palaeoclimatology Palaeoecology*, v. 156, p. 243-259.
- Thomas, D.S.G., Brook, G., Shaw, P., Bateman, M., Appleton, C., Nash, D., McLaren, S., and Davies, F., 2003, Late Pleistocene wetting and drying in the NW Kalahari: an integrated study from the Tsodilo Hills, Botswana: *Quaternary International*, v. 104, p. 53-67.
- Wellington, J.H., 1955, *Southern Africa Volume I Physical Geography*: Cambridge, Cambridge University Press, p. 588-591.

White, K., Eckardt, F., 2006, Geochemical mapping of carbonate sediments in the Makgadikgadi basin, Botswana using moderate resolution remote sensing data: *Earth Surface Processes and Landforms*, v. 31, p. 665–681.

APPENDICES

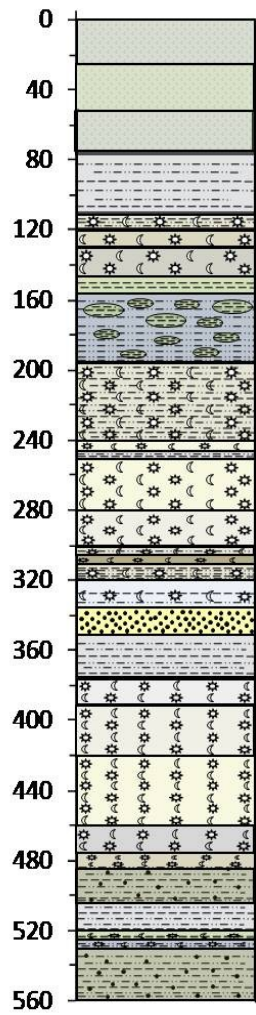
A1: MabX Lithologic Section
A2: MabX Physical Properties
A3: MabX Organic Matter and Carbonate
A4: MabX Metals Presented in Text
A5: MabX Additional Metals


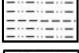
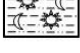
B1: Mab6 Physical Properties
B2: Mab6 Organic Matter and Carbonate
B3: Mab6 Metals Presented in Text
B4: Mab6 Additional Metals


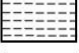

C1: XRD Results



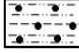
APPENDIX A1

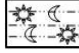
MabX Lithologic Section



 **Organic-rich Sediment**
 **Clayey-Silt**
 **Diatomaceous Clayey-Silt**

 **Diatomite**
 **Clay**
 **Silt with Clay Clasts**

 **Clayey-Silty Diatomite**
 **Sand**
 **Sandy Clay Silt**

 **Clayey Diatomite**
 **Silty Diatomite**

APPENDIX A2

MabX Physical Properties

Sample Depth (cm)	X_{hf} (m ³ /kg)	Graphic Mean Φ	Sand (%)	Silt (%)	Clay (%)	Sorting (SD)	Skewness	Description
5	7.31E-08	7.27	0.2	63.7	36.1	1.63	0.01	organic-rich silt
10	6.24E-08	6.91	2.3	68.0	29.7	1.74	0.02	organic-rich silt
15	7.51E-08	7.44	0.1	60.6	39.3	1.63	-0.01	organic-rich silt
20	7.68E-08	7.40	0.1	60.8	39.0	1.63	-0.03	organic-rich silt
25	7.57E-08	7.61	0.0	57.7	42.3	1.46	-0.07	organic-rich clayey-silt
30	7.94E-08	7.64	0.0	57.1	42.9	1.42	-0.08	organic-rich clayey-silt
35	7.92E-08	7.56	0.0	58.3	41.7	1.53	-0.05	organic-rich clayey-silt
40	7.60E-08	7.64	0.0	57.1	42.9	1.45	-0.06	organic-rich clayey-silt
45	7.70E-08	7.61	0.0	57.6	42.4	1.48	-0.06	organic-rich clayey-silt
50	7.67E-08	7.35	0.1	62.9	37.0	1.61	0.04	organic-rich silt
55	7.71E-08	7.44	0.0	61.4	38.6	1.55	0.02	organic-rich silt
60	7.32E-08	7.31	0.0	64.6	35.4	1.56	0.06	organic-rich silt
65	7.50E-08	7.39	0.0	62.9	37.1	1.54	0.04	organic-rich silt
70	7.44E-08	7.36	0.0	64.5	35.5	1.47	0.03	organic-rich silt
75	7.72E-08	7.43	0.0	63.4	36.6	1.41	0.03	organic-rich silt
80	7.36E-08	7.22	0.0	67.8	32.2	1.50	0.10	clayey-silt
85	6.89E-08	7.15	0.0	70.8	29.2	1.46	0.14	clayey-silt
90	5.90E-08	6.97	0.1	74.9	25.0	1.48	0.14	clayey-silt
95	6.43E-08	7.03	0.2	71.2	28.7	1.57	0.10	clayey-silt
100	5.76E-08	6.95	0.2	74.7	25.2	1.50	0.11	clayey-silt
105	6.00E-08	6.82	2.0	72.6	25.4	1.67	0.08	clayey-silt
110	7.19E-08	6.74	0.2	79.6	20.2	1.47	0.17	diatomaceous clayey-silt
115	7.68E-08	6.93	0.1	77.0	22.9	1.40	0.09	diatomaceous clayey-silt
120	5.56E-08	6.59	0.2	83.4	16.5	1.35	0.13	light-brown diatomite
125	5.59E-08	6.80	0.1	79.2	20.7	1.44	0.15	light-brown diatomite

Sample Depth (cm)	X_{hf} (m ³ /kg)	Graphic Mean Φ	Sand (%)	Silt (%)	Clay (%)	Sorting (SD)	Skewness	Description
130	5.10E-08	6.52	0.1	85.9	14.0	1.26	0.15	light-brown gray diatomite
140	4.23E-08	6.45	1.7	82.3	16.0	1.48	0.17	light-brown gray diatomite
145	6.98E-08	7.45	0.0	62.5	37.5	1.43	-0.03	clay
150	6.93E-08	7.48	0.0	63.5	36.5	1.32	0.01	clay
155	6.36E-08	7.21	0.0	69.3	30.7	1.42	0.06	silt with clay clasts
160	6.24E-08	7.22	0.0	69.5	30.5	1.41	0.05	silt with clay clasts
165	6.55E-08	7.03	1.3	69.8	28.8	1.58	0.05	silt with clay clasts
170	6.90E-08	7.00	0.1	74.2	25.7	1.47	0.11	silt with clay clasts
175	6.85E-08	6.87	0.2	74.4	25.4	1.56	0.09	silt with clay clasts
180	6.63E-08	6.89	0.1	76.1	23.8	1.49	0.14	silt with clay clasts
185	6.84E-08	6.76	0.1	78.1	21.8	1.53	0.20	silt with clay clasts
190	5.47E-08	6.72	0.1	80.5	19.4	1.41	0.15	silt with clay clasts
195	6.41E-08	6.83	0.0	78.3	21.7	1.44	0.18	diatomaceous clayey-silt
200	6.21E-08	6.75	0.0	78.7	21.2	1.54	0.23	diatomaceous clayey-silt
205	6.67E-08	6.76	0.1	77.6	22.3	1.56	0.19	diatomaceous clayey-silt
210	7.35E-08	6.84	0.0	75.7	24.3	1.56	0.19	diatomaceous clayey-silt
215	7.15E-08	6.93	0.0	75.8	24.2	1.46	0.14	diatomaceous clayey-silt
220	8.11E-08	6.96	0.0	75.4	24.5	1.45	0.13	diatomaceous clayey-silt
225	8.30E-08	6.91	0.0	76.4	23.6	1.46	0.19	diatomaceous clayey-silt
230	8.96E-08	6.88	0.0	77.4	22.6	1.45	0.22	diatomaceous clayey-silt
235	8.42E-08	6.83	0.0	77.1	22.9	1.53	0.26	diat. clayey-silt, gastropds
240	4.43E-08	6.67	0.2	76.2	23.6	1.70	0.28	white diatomite
245	5.56E-08	6.54	0.2	82.4	17.4	1.50	0.23	clayey-silt
250	3.69E-08	6.75	0.2	74.3	25.6	1.70	0.31	white diatomite

Sample Depth (cm)	X_{hf} (m ³ /kg)	Graphic Mean Φ	Sand (%)	Silt (%)	Clay (%)	Sorting (SD)	Skewness	Description
255	3.66E-08	6.58	0.2	78.7	21.1	1.66	0.35	white diatomite
265	3.90E-08	6.31	0.2	84.9	14.9	1.48	0.32	white diatomite
270	5.26E-08	6.23	0.2	87.6	12.2	1.28	0.23	white diatomite
275	5.35E-08	6.13	0.2	89.3	10.5	1.22	0.20	white diatomite
280	5.62E-08	6.31	0.2	86.4	13.5	1.34	0.23	white diatomite
285	6.66E-08	6.50	0.2	82.6	17.2	1.52	0.26	light-tan diatomite
290	6.14E-08	6.37	1.3	82.9	15.8	1.60	0.26	light-tan diatomite
295	5.67E-08	6.31	3.8	80.5	15.7	1.62	0.21	light-tan diatomite
300	7.91E-08	6.89	0.0	77.0	22.9	1.43	0.12	diatomaceous clayey-silt
305	9.70E-08	6.61	0.0	83.4	16.6	1.31	0.21	brown diatomite
310	1.02E-07	6.82	0.0	75.8	24.2	1.54	0.23	diatomaceous clayey-silt
315	8.95E-08	6.75	0.0	77.5	22.5	1.51	0.22	diatomaceous clayey-silt
320	7.56E-08	6.46	0.1	82.5	17.4	1.53	0.33	clayey-silty diatomite
325	7.65E-08	6.65	0.0	80.4	19.6	1.46	0.25	clayey-silty diatomite
330	7.58E-08	6.68	0.0	80.1	19.9	1.45	0.28	clayey-silty diatomite
335	8.25E-08	6.75	1.7	75.1	23.2	1.62	0.18	sand
340	5.42E-08	5.88	23.0	60.0	17.0	2.13	0.03	sand
345	2.84E-08	4.76	48.3	42.0	9.7	1.91	0.52	sand
350	6.13E-08	6.51	4.0	77.8	18.2	1.62	0.17	clayey-silt
355	7.22E-08	6.57	1.2	80.1	18.6	1.56	0.23	clayey-silt
360	7.52E-08	6.79	0.1	79.3	20.6	1.41	0.17	clayey-silt
365	8.21E-08	6.77	0.8	77.7	21.6	1.50	0.11	clayey-silt
370	8.43E-08	6.76	0.1	78.7	21.1	1.46	0.14	clayey-silt
375	4.80E-08	5.96	0.2	91.5	8.3	1.15	0.33	white-gray diatomite
380	3.67E-08	6.00	0.1	92.3	7.6	1.11	0.31	white-gray diatomite

Sample Depth (cm)	X_{hf} (m ³ /kg)	Graphic Mean Φ	Sand (%)	Silt (%)	Clay (%)	Sorting (SD)	Skewness	Description
385	3.77E-08	5.88	0.4	92.4	7.2	1.14	0.30	white-gray diatomite
395	7.76E-08	6.37	0.0	85.4	14.6	1.43	0.42	light-tan diatomite
400	8.38E-08	6.35	0.0	85.6	14.4	1.45	0.44	light-tan diatomite
405	8.19E-08	6.39	0.0	85.3	14.7	1.43	0.42	light-tan diatomite
410	7.98E-08	6.27	0.0	86.9	13.1	1.29	0.39	light-tan diatomite
415	6.85E-08	6.25	0.1	86.5	13.3	1.33	0.36	light-tan diatomite
420	5.91E-08	6.18	0.0	88.6	11.4	1.21	0.41	white diatomite
425	5.50E-08	6.20	0.0	88.6	11.4	1.20	0.41	white diatomite
430	6.18E-08	6.31	0.0	87.1	12.9	1.24	0.37	white diatomite
435	6.91E-08	6.45	0.0	85.9	14.1	1.25	0.30	white diatomite
440	5.96E-08	6.32	0.0	87.6	12.4	1.21	0.32	white diatomite
445	5.96E-08	6.26	0.0	88.2	11.8	1.20	0.41	white diatomite
450	5.40E-08	6.42	0.0	86.7	13.3	1.22	0.34	white diatomite
455	6.11E-08	6.41	0.0	86.4	13.6	1.24	0.36	white diatomite
460	4.35E-08	6.10	0.1	89.8	10.1	1.19	0.37	light-gray diatomite
465	5.22E-08	6.00	0.0	90.2	9.7	1.18	0.42	light-gray diatomite
470	6.06E-08	6.13	0.1	88.2	11.7	1.28	0.39	light-gray diatomite
475	7.50E-08	6.51	0.1	82.0	17.9	1.55	0.37	light-brown diatomite
480	8.33E-08	6.86	0.1	75.3	24.6	1.57	0.24	light-brown diatomite
485	7.14E-08	6.61	2.1	77.4	20.5	1.66	0.26	sandy-clay silt
490	6.87E-08	6.34	11.2	70.2	18.7	1.97	0.06	sandy-clay silt
495	6.51E-08	6.25	12.7	69.0	18.3	2.00	0.05	sandy-clay silt
500	7.83E-08	6.62	3.3	76.3	20.4	1.64	0.22	sandy-clay silt
505	1.04E-07	6.85	0.0	77.2	22.8	1.46	0.33	clayey-silt
510	9.72E-08	6.74	0.1	77.9	22.0	1.56	0.26	clayey-silt

Sample Depth (cm)	X_{hf} (m ³ /kg)	Graphic Mean Φ	Sand %	Silt %	Clay %	Sorting (SD)	Skewness	Description
515	1.19E-07	7.02	0.0	74.3	25.7	1.44	0.21	clayey-silt
525	8.32E-08	6.33	0.2	84.8	15.0	1.53	0.32	silty diatomite
530	7.38E-08	6.22	2.8	82.3	14.9	1.63	0.26	sandy-clay silt
535	7.39E-08	6.01	10.1	75.6	14.3	1.79	0.19	sandy-clay silt
540	7.57E-08	6.21	3.3	82.1	14.7	1.62	0.27	sandy-clay silt
550	9.14E-08	6.21	4.8	76.0	19.3	1.62	0.27	sandy-clay silt
560	8.19E-08	6.31	4.5	79.2	16.3	1.69	0.22	sandy-clay silt

APPENDIX A3

MabX Carbonate and Organic Matter

Sample Depth (cm)	Carbonate (%)	Organic Matter (%)
5	0.002	1.47
10	0.005	2.58
15	0.002	1.28
20	0.003	1.37
25	0.000	1.20
30	0.001	1.20
35	0.002	1.17
40	0.003	1.08
45	0.010	1.13
50	0.002	0.98
55	0.001	0.98
60	0.001	0.98
65	0.000	0.97
70	0.000	0.95
75	0.002	0.86
80	0.007	0.85
85	0.020	0.85
90	0.003	0.92
95	0.001	1.09
100	0.000	0.61
105	0.002	1.26
110	0.004	0.45
115	0.006	0.52
120	0.029	0.33
125	0.002	0.53
130	0.086	0.25
135	0.004	0.35
140	0.076	0.43
145	0.001	0.93
150	0.003	0.91
155	0.004	0.64
160	0.015	0.63
165	0.010	0.54
170	0.046	0.41
175	0.002	0.34
180	0.073	0.27
185	0.008	0.20
190	0.056	0.26
195	0.008	0.16
200	0.107	0.11

Sample Depth (cm)	Carbonate (%)	Organic Matter (%)
205	0.910	0.45
210	0.645	0.26
215	0.110	0.44
220	0.009	0.52
225	0.059	0.38
230	0.041	0.36
235	0.754	0.24
240	3.343	0.28
245	1.387	0.44
250	3.490	0.24
255	2.626	0.39
260	1.139	0.27
265	0.498	1.47
270	0.239	0.09
275	0.059	0.24
280	0.138	0.09
285	0.049	0.17
290	0.018	0.15
295	0.024	0.18
300	0.072	0.17
305	0.028	0.39
310	0.010	0.26
315	0.030	0.25
320	0.127	0.22
325	0.004	0.20
330	0.003	0.21
335	0.004	0.34
340	0.001	0.28
345	0.003	0.15
350	0.010	0.39
355	0.016	0.40
360	0.008	0.37
365	0.003	0.43
370	0.013	0.37
375	0.008	0.29
380	0.007	0.21
385	0.003	0.20
390	3.245	0.42
395	0.020	0.28
400	0.003	0.27

Sample Depth (cm)	Carbonate (%)	Organic Matter (%)
405	0.003	0.25
410	0.006	0.27
415	0.005	0.21
420	0.003	0.20
425	0.004	0.22
430	0.005	0.24
435	0.002	0.22
440	0.002	0.22
445	0.012	0.18
450	0.001	0.21
455	0.002	0.20
460	0.001	0.18
465	0.003	0.22
470	0.003	0.21
475	0.017	0.24
480	0.021	0.31
485	0.002	0.22
490	0.023	0.20
495	0.003	0.19
500	0.002	0.23
505	0.002	0.23
510	0.003	0.26
515	0.158	0.25
520	0.116	0.20
525	0.004	0.29
530	0.010	0.31
535	0.006	0.27
540	0.003	0.23
550	0.007	0.27
560	0.006	0.29

APPENDIX A4

MabX Metals Presented in Text

Sample Depth (cm)	Li (ppm)	K (ppm)	Rb (ppm)	Mg (ppm)	Cs (ppm)	Ca (wt. %)	Sr (ppm)	Ba (ppm)	Al (wt. %)	V (ppm)	Cr (ppm)	Mn (ppm)	Fe (wt. %)	Co ppm	Ni ppm	Cu ppm	Zn ppm
5	31	6709	310	4903	215	0.5	360	225	5.8	160	99	136	2.7	73	45	65	12
10	22	6425	282	4092	193	0.5	302	200	4.6	133	88	102	2.3	64	37	60	10
15	34	7818	322	5496	227	0.6	393	226	6.7	169	110	137	3.3	72	54	66	32
20	32	7323	320	5280	213	0.5	384	221	6.4	169	107	121	3.0	73	53	67	16
25	34	6713	277	4985	213	0.5	358	214	6.2	156	96	144	3.1	64	61	73	32
30	34	7193	276	5201	211	0.5	363	217	5.6	159	97	138	3.0	64	48	56	7
35	34	6682	284	4954	216	0.5	360	213	6.2	160	98	136	3.0	66	65	68	31
40	35	6381	266	5160	224	0.5	344	232	5.7	161	96	144	3.0	61	141	83	47
45	34	6581	267	5247	212	0.5	353	219	5.3	153	90	136	2.9	60	56	75	21
50	36	6593	287	5424	413	0.6	383	403	6.0	176	98	136	2.9	67	49	60	10
55	36	6179	276	5342	225	0.6	366	225	5.4	172	97	171	3.1	65	63	63	43
60	35	6576	289	5325	236	0.6	358	232	5.6	174	102	161	3.2	65	121	74	68
65	36	6659	280	5518	243	0.6	386	253	5.7	170	104	150	3.1	64	75	64	27
70	36	7066	285	5638	256	0.6	395	257	5.5	169	100	147	2.9	65	58	69	22
75	36	7031	259	5557	280	0.7	385	272	5.4	170	94	177	3.3	60	49	62	14
80	32	6610	293	5426	228	0.6	387	244	6.2	168	105	140	3.2	71	57	63	-
85	26	6425	255	5066	257	0.7	341	259	4.7	149	84	128	2.6	58	51	56	15
90	19	5018	217	3790	215	0.5	288	227	4.3	130	75	119	2.4	52	151	101	122
95	21	4648	230	3861	238	0.6	280	246	4.3	124	78	95	2.3	54	193	257	316
100	20	4938	297	4237	334	0.5	332	329	4.5	156	92	94	2.4	70	97	180	173
105	23	5328	281	4408	264	0.6	339	282	5.1	155	95	106	2.5	65	54	87	50
110	16	4597	253	4131	424	0.5	323	431	4.3	142	84	71	2.5	61	79	109	142
115	18	5034	269	4569	271	0.5	334	276	4.7	159	96	88	2.7	65	218	222	222
120	15	4795	273	4437	224	0.7	319	225	4.0	151	91	70	2.4	66	41	55	-
125	19	5305	263	4667	196	0.5	326	200	4.4	150	86	93	2.5	62	76	84	30
130	15	4463	254	3976	191	0.9	272	199	3.4	142	78	72	2.1	61	46	62	10
135	13	4449	277	3912	172	0.4	278	185	3.5	144	83	62	2.1	67	42	58	-

A4-3

Sample	Li	K	Rb	Mg	Cs	Ca	Sr	Ba	Al	V	Cr	Mn	Fe	Co	Ni	Cu	Zn
Depth (cm)	(ppm)	(ppm)	(ppm)	(ppm)	(ppm)	(wt. %)	(ppm)	(ppm)	(wt. %)	(ppm)	(ppm)	(ppm)	(wt. %)	(ppm)	(ppm)	(ppm)	(ppm)
140	16	4638	281	3823	230	0.6	285	235	3.8	152	90	97	2.3	70	45	74	18
145	33	6870	285	5291	251	0.5	376	253	6.4	167	110	145	3.0	66	59	70	21
150	35	7054	295	5323	237	0.4	365	232	6.7	177	103	142	3.1	69	195	128	44
155	23	5248	286	4455	189	0.5	323	193	4.8	136	94	103	2.6	68	56	114	52
160	19	4354	234	3490	165	0.6	249	165	3.9	126	74	104	1.9	57	133	107	729
165	26	5450	281	4555	219	0.4	344	218	5.2	167	93	156	2.7	66	54	72	30
170	24	5937	281	5360	228	0.7	360	228	5.1	162	94	161	2.8	69	67	117	55
175	20	6588	295	5492	182	0.4	347	182	4.5	156	92	147	2.8	70	49	67	2
180	20	6392	295	5496	217	0.6	349	210	4.6	165	94	158	2.8	69	63	106	30
185	21	7095	292	5917	198	0.5	358	204	4.5	174	101	152	3.0	70	62	71	21
190	12	4607	269	4079	137	1.0	246	145	3.0	137	81	92	1.8	66	273	332	206
195	22	6854	289	5726	194	3.8	367	203	4.6	172	103	137	3.1	70	71	72	36
200	22	6363	281	5969	158	2.6	354	160	4.6	178	103	174	3.0	66	71	128	83
205	24	5575	270	5939	296	1.0	464	286	4.6	161	99	297	3.1	66	64	168	348
210	24	5880	300	5780	255	0.6	429	248	4.8	178	103	213	2.8	72	92	184	360
215	22	6280	309	5691	251	0.9	407	246	4.6	190	103	190	3.5	73	50	112	52
220	25	7698	306	6229	204	0.7	394	210	4.7	174	97	202	3.3	69	51	115	80
225	25	7191	306	6478	236	3.9	442	232	5.2	184	101	210	3.5	72	50	77	22
230	27	7178	305	6805	297	11.9	475	298	5.1	163	101	217	3.8	71	42	89	204
235	26	6530	296	6524	320	5.4	548	317	5.0	179	95	234	3.4	70	55	89	474
240	13	3511	258	6434	878	12.4	887	835	2.8	110	73	349	1.8	63	51	174	175
245	11	4712	266	5589	559	8.6	557	527	2.7	121	73	196	2.2	64	52	108	18
250	12	3682	276	7045	901	3.8	822	836	2.7	106	78	468	1.7	64	30	67	-
255	49	2997	200	4708	498	6.7	466	470	2.1	107	66	395	1.5	55	33	50	1
260	41	3525	220	4108	303	1.1	314	244	2.8	143	77	164	1.7	62	34	58	11
265	47	3743	224	4647	361	0.6	383	296	3.1	133	78	335	1.9	61	30	51	-
270	44	4337	224	4225	191	0.6	268	117	3.7	166	88	103	2.4	64	37	53	0

Sample	Li	K	Rb	Mg	Cs	Ca	Sr	Ba	Al	V	Cr	Mn	Fe	Co	Ni	Cu	Zn
Depth (cm)	(ppm)	(ppm)	(ppm)	(ppm)	(ppm)	(wt. %)	(ppm)	(ppm)	(wt. %)	(ppm)	(ppm)	(ppm)	(wt. %)	(ppm)	(ppm)	(ppm)	(ppm)
275	41	4461	212	4337	195	0.4	264	136	3.7	163	85	88	2.5	59	36	50	-
280	41	5532	230	4744	200	0.7	280	137	3.9	168	90	93	2.5	65	37	52	0
285	46	4815	221	4792	189	0.7	303	119	4.6	184	96	123	3.0	64	39	52	-
290	45	4355	233	4351	183	1.1	280	108	4.3	185	95	102	2.7	68	39	54	-
295	46	3940	234	3770	181	0.6	233	94	4.0	184	95	89	2.5	69	62	116	296
300	71	4255	241	4940	224	0.9	349	133	5.7	229	112	134	3.5	74	54	74	18
305	41	5051	222	5221	408	0.5	411	338	5.0	198	98	190	3.9	67	54	93	38
310	64	5078	250	5821	223	0.4	442	156	5.9	237	112	241	4.3	74	49	67	15
315	57	4510	223	5102	197	0.5	377	135	5.6	211	106	189	3.6	66	42	51	-
320	50	4516	266	5021	156	0.3	387	167	6.7	221	105	193	3.3	67	44	57	-
325	27	4590	227	4612	138	0.2	291	116	5.6	133	48	161	2.9	-	14	-	28
330	39	5197	284	4898	160	0.4	366	170	6.0	201	104	132	3.1	68	43	65	65
335	27	5254	275	4711	186	0.5	375	195	5.1	176	98	139	3.2	69	56	91	72
340	17	3176	228	2986	120	0.4	273	132	3.3	126	74	92	2.2	57	37	65	47
345	6	1522	246	1411	72	0.4	168	83	1.5	98	66	16	1.1	60	33	65	34
350	23	3013	269	3050	143	0.5	298	153	3.6	143	88	82	2.4	66	59	102	87
355	28	4261	275	4162	183	0.3	384	191	5.5	156	98	133	3.2	70	44	67	11
360	25	3709	244	3773	157	0.3	360	167	4.6	153	90	121	3.1	64	40	60	35
365	26	4360	262	4081	192	0.3	411	197	4.8	160	96	154	3.5	67	45	67	11
370	28	4474	247	4138	195	5.6	409	190	5.2	169	92	153	3.5	62	44	72	81
375	15	2662	257	2544	106	0.6	243	115	2.8	135	81	209	1.8	66	35	68	7
380	11	2367	244	2302	91	0.4	204	97	2.5	128	74	44	1.4	62	35	68	43
385	14	2294	251	2311	87	0.4	214	93	2.7	130	78	48	1.5	64	33	54	9
390	33	3625	255	3881	224	0.5	377	213	5.5	151	100	771	2.8	68	40	58	17
395	41	3944	244	4165	155	0.4	368	149	5.5	168	100	142	3.2	61	41	52	10
400	41	4037	272	4402	148	0.4	375	149	6.2	181	107	108	3.4	70	192	117	135
405	43	3987	282	4417	146	0.3	391	147	6.2	186	110	108	3.3	70	51	110	24

A4-5

Sample Depth (cm)	Li (ppm)	K (ppm)	Rb (ppm)	Mg (ppm)	Cs (ppm)	Ca (wt. %)	Sr (ppm)	Ba (ppm)	Al (wt. %)	V (ppm)	Cr (ppm)	Mn (ppm)	Fe (wt. %)	Co (ppm)	Ni (ppm)	Cu (ppm)	Zn (ppm)
410	37	3714	257	4153	138	0.4	374	141	5.9	175	101	100	3.3	66	45	57	-
415	37	3415	239	3643	131	0.3	333	135	5.5	154	87	87	2.7	61	39	52	-
420	32	3416	257	3810	126	0.3	320	133	4.9	148	91	70	2.3	66	39	57	91
425	29	3353	256	3653	128	0.3	311	131	4.8	156	89	71	2.4	66	38	61	20
430	26	3168	269	3505	122	0.3	305	128	4.4	147	86	55	2.2	66	35	73	6
435	28	2832	264	3261	121	0.4	339	126	4.4	148	81	55	2.5	65	36	57	2
440	30	2965	234	3348	127	0.4	310	131	4.5	146	82	69	2.7	61	40	60	28
445	33	3118	277	3292	129	0.5	323	130	5.1	161	94	63	2.7	71	47	66	11
450	28	3085	276	3037	123	0.5	274	130	4.4	154	89	41	2.3	67	203	174	121
455	32	3207	250	3174	124	0.8	274	131	5.0	162	92	68	2.4	62	153	175	234
460	28	2600	245	2530	104	0.4	231	108	4.0	158	83	48	1.8	64	40	67	31
465	39	3102	255	3211	127	0.5	290	130	5.5	177	99	71	2.4	66	44	68	21
470	36	3258	245	3545	142	0.4	322	146	5.7	171	93	95	2.6	63	44	72	187
475	50	3609	264	3819	169	0.7	374	165	6.1	210	110	135	3.3	69	67	84	56
480	55	3930	272	4114	221	0.5	405	214	6.7	218	116	162	3.6	70	49	69	18
485	65	4522	296	4435	238	1.0	410	226	7.6	241	127	168	3.7	80	54	68	257
490	39	3742	271	3641	232	0.8	327	229	6.1	189	103	161	2.8	70	43	63	212
495	51	4588	254	4099	246	0.5	384	235	7.4	199	103	197	3.4	66	45	56	202
500	47	4172	269	4016	244	0.4	387	231	5.7	198	103	150	3.5	71	47	145	25
505	52	4629	270	4522	256	0.7	451	246	7.8	215	108	228	4.1	71	48	63	28
510	55	4717	297	4425	212	0.5	434	210	6.8	222	118	170	3.9	80	52	69	113
515	60	4673	287	4933	232	1.0	519	218	5.2	237	121	219	5.1	80	54	78	244
520	61	5245	283	5336	246	0.8	544	232	5.5	237	121	251	4.9	76	51	66	213
525	48	4214	277	3988	172	0.5	368	168	6.4	199	109	130	3.3	72	51	64	74
530	37	3790	277	3929	169	0.5	369	162	6.3	195	114	148	3.3	74	45	60	61
535	35	3510	293	3676	180	0.4	360	177	5.8	190	110	165	3.0	76	47	64	81
540	40	3648	277	3637	159	0.4	369	158	6.1	184	105	163	3.0	73	45	58	75

Sample	Li	K	Rb	Mg	Cs	Ca	Sr	Ba	Al	V	Cr	Mn	Fe	Co	Ni	Cu	Zn
Depth (cm)	(ppm)	(ppm)	(ppm)	(ppm)	(ppm)	(wt. %)	(ppm)	(ppm)	(wt. %)	(ppm)	(ppm)	(ppm)	(wt. %)	(ppm)	(ppm)	(ppm)	(ppm)
550	40	4058	281	4146	197	0.5	432	193	6.6	193	115	207	3.8	76	48	59	55
560	29	3750	262	4052	159	0.5	383	156	5.7	187	114	180	3.3	74	50	63	205

- Indicates not detected by analysis

APPENDIX A5

MabX Additional Metals

Sample Depth (cm)	Na (ppm)	Ag (ppm)	Cd (ppm)	Pb (ppm)	Ga (ppm)
5	161	18	25	22	175
10	107	18	23	28	150
15	144	13	24	23	187
20	152	12	25	29	188
25	171	8	20	30	169
30	160	7	20	22	174
35	198	8	20	22	170
40	195	4	19	29	169
45	225	9	19	20	161
50	256	11	21	24	177
55	254	15	20	32	146
60	279	8	21	18	175
65	283	6	20	29	186
70	296	5	20	20	186
75	300	6	18	27	163
80	293	12	22	19	174
85	298	7	19	24	161
90	192	10	16	24	125
95	236	10	18	33	130
100	226	16	25	36	168
105	233	16	23	29	162
110	229	14	21	33	152
115	257	12	21	41	162
120	203	15	23	29	167
125	229	10	21	42	160
130	191	13	22	27	150
135	184	16	24	24	160
140	202	15	24	31	168
145	185	9	22	42	178
150	248	15	22	41	171
155	234	14	24	25	173
160	325	12	18	39	135
165	207	12	23	32	176
170	212	11	22	24	174
175	249	15	24	34	187
180	238	14	23	23	178
185	264	11	22	38	181
190	221	17	23	43	147
195	260	9	22	31	180
200	325	9	21	39	170

Sample Depth (cm)	Na (ppm)	Ag (ppm)	Cd (ppm)	Pb (ppm)	Ga (ppm)
205	732	12	21	109	157
210	1111	17	24	58	177
215	657	15	24	34	178
220	871	12	23	37	168
225	503	8	23	25	175
230	385	11	23	56	170
235	381	10	22	78	174
240	939	17	25	55	143
245	617	18	23	27	145
250	376	19	25	29	150
255	462	15	20	22	123
260	221	14	22	20	145
265	250	16	23	39	143
270	236	15	22	44	149
275	236	11	20	35	155
280	613	11	22	44	168
285	335	10	22	53	175
290	299	10	24	50	185
295	264	12	25	84	183
300	294	7	22	25	203
305	384	8	20	30	166
310	820	9	22	62	192
315	391	4	20	44	178
320	628	6	21	53	191
325	304	-	-	-	-
330	240	8	23	41	193
335	276	8	23	51	189
340	144	12	20	49	140
345	96	17	24	54	142
350	352	14	24	37	171
355	339	8	22	28	189
360	196	8	21	49	161
365	203	7	21	35	173
370	238	6	20	33	185
375	149	16	24	58	171
380	547	11	24	48	166
385	193	12	24	48	167
390	290	8	22	53	190
395	270	3	18	26	188
400	257	6	21	42	200

Sample Depth (cm)	Na (ppm)	Ag (ppm)	Cd (ppm)	Pb (ppm)	Ga (ppm)
405	315	8	22	34	190
410	621	6	21	45	184
415	325	6	20	40	173
420	354	11	21	53	176
425	267	9	22	53	174
430	191	15	24	41	168
435	204	17	23	25	157
440	206	11	20	50	153
445	206	14	25	64	170
450	255	15	23	44	161
455	328	11	21	44	160
460	191	15	23	55	150
465	218	11	23	47	174
470	210	8	20	60	165
475	270	10	22	54	174
480	263	4	21	36	200
485	572	3	24	60	227
490	456	7	23	65	193
495	580	0	20	46	204
500	307	9	22	23	184
505	269	1	21	57	197
510	351	2	24	63	233
515	518	-	21	60	208
520	527	-	19	30	225
525	334	4	22	23	204
530	280	2	23	31	211
535	274	8	25	35	211
540	299	8	22	26	208
550	284	7	22	15	202

- Not detected in sample

97

APPENDIX B1

Mab6 Physical Properties

Sample Depth (cm)	X_{hf}	Graphic Mean Φ	Sand (%)	Silt (%)	Clay (%)	Sorting (SD)	Skewness
20	6.09E-08	7.21	3.8	64.2	32.0	1.59	-0.09
40	5.68E-08	7.17	1.9	69.2	28.9	1.47	-0.01
60	6.02E-08	7.25	0.8	68.1	31.0	1.45	-0.01
80	5.83E-08	6.98	2.8	68.5	28.6	1.66	0.04
100	5.31E-08	6.88	1.7	73.4	24.8	1.57	0.09
120	4.92E-08	6.95	0.9	75.3	23.8	1.45	0.06
140	4.10E-08	6.24	12.8	67.3	20.0	1.93	0.01
160	4.24E-08	6.90	1.2	74.7	24.0	1.52	-0.01
180	3.89E-08	6.73	0.2	76.7	23.1	1.63	0.15
200	2.79E-08	5.87	3.1	88.4	8.5	1.34	0.16
220	3.14E-08	6.99	0.0	70.1	29.9	1.65	0.17
240	5.12E-08	6.87	0.1	76.1	23.8	1.52	0.12
260	6.01E-08	6.79	0.1	76.4	23.5	1.59	0.19
280	4.47E-08	7.11	0.0	66.7	33.3	1.71	0.21
300	9.46E-08	5.89	3.0	88.3	8.7	1.34	0.16
320	1.06E-07	5.92	1.7	90.3	8.0	1.26	0.17
340	9.28E-08	6.51	0.0	85.8	14.2	1.24	0.23
360	8.51E-08	6.64	0.1	83.2	16.7	1.31	0.15
380	7.98E-08	6.67	3.1	76.7	20.3	1.56	0.07
400	6.55E-08	6.44	11.4	68.2	20.3	1.86	-0.03
420	7.32E-08	6.69	2.5	77.4	20.1	1.51	0.09
440	4.45E-08	5.89	1.4	90.1	8.5	1.22	0.30

APPENDIX B2

Mab6 Carbonate and Organic Matter

Sample Depth (cm)	Carbonate (%)	Organic Matter (%)
20	0.007	1.52
40	0.333	0.84
60	0.202	0.67
80	0.495	0.63
100	0.465	0.46
120	0.488	0.40
140	0.580	0.38
160	0.341	0.62
180	2.986	0.24
200	6.091	0.45
220	5.085	0.42
240	1.791	0.43
260	1.645	0.46
280	4.649	0.41
300	0.155	0.11
320	0.537	1.52
340	0.070	0.44
360	0.122	0.38
380	0.042	0.50
400	0.138	0.28
420	0.064	0.35
440	0.041	0.23

APPENDIX B3

Mab6 Metals Presented in Text

B3-2

Sample Depth (cm)	Li (ppm)	K (ppm)	Rb (ppm)	Mg (ppm)	Cs (ppm)	Ca (wt. %)	Sr (ppm)	Ba (ppm)	Al (wt. %)	V (ppm)	Cr (ppm)	Mn (ppm)	Fe (wt. %)	Co (ppm)	Ni (ppm)	Cu (ppm)	Zn (ppm)
20	26	5968	289	4632	194	0.5	325	193	4.8	147	96	115	2.5	70	44	61	119
40	25	6229	288	5915	214	1.0	373	213	4.9	158	92	52	2.2	70	40	62	61
60	28	6522	278	5408	245	0.9	363	232	5.0	164	93	86	2.5	68	40	60	49
80	20	5624	274	4654	320	1.8	347	311	4.0	153	84	78	2.1	66	33	67	9
100	19	4959	273	4033	242	1.6	315	234	3.7	148	83	69	2.0	67	36	57	1
120	19	4801	269	3975	330	1.9	327	323	3.8	149	85	106	2.1	66	37	57	61
140	11	3644	265	3263	225	2.9	335	219	2.7	122	76	170	1.6	66	35	57	5
160	7	3721	266	3318	226	1.7	293	217	2.0	107	69	90	1.5	65	29	58	20
180	10	3477	256	4609	359	10.1	650	338	2.4	103	71	424	1.6	62	32	62	18
200	6	2326	234	6076	664	12.3	918	597	1.7	68	65	1284	1.0	59	27	39	-
220	8	2456	262	5979	489	9.9	700	438	2.2	95	77	1055	1.2	68	31	47	33
240	18	4577	278	5172	302	7.5	466	283	4.1	144	89	318	2.3	69	47	75	81
260	18	5339	291	5588	442	6.4	600	406	3.7	140	87	247	2.6	72	40	58	39
280	10	3229	277	5851	890	15.5	835	776	2.0	102	76	847	1.7	68	30	48	-
300	4	5640	232	4531	1115	1.4	447	1015	2.2	111	67	101	3.4	67	36	54	55
320	3	4890	257	4271	720	2.4	451	663	2.1	130	71	86	3.3	70	35	51	45
340	23	5318	259	5240	254	1.3	426	245	5.5	181	98	137	3.8	69	52	74	54
360	19	6098	273	5445	249	1.6	440	247	4.7	185	98	144	3.6	73	46	68	49
380	20	4090	246	3754	224	0.6	394	217	4.4	159	87	130	3.5	65	44	64	31
400	20	3113	253	3278	259	1.5	324	247	3.9	150	87	121	2.4	66	38	53	-
420	25	3535	246	3660	217	0.9	320	207	4.5	172	93	118	2.6	64	44	62	57
440	21	2861	232	2791	127	0.4	251	124	3.7	160	80	1	2.0	61	37	54	38

- Not detected in sample

APPENDIX B4

Mab6 Additional Metals

Sample Depth (cm)	Na (ppm)	Ag (ppm)	Cd (ppm)	Pb (ppm)	Ga (ppm)
20	277	14	24	57	168
40	677	15	25	56	167
60	484	15	23	58	155
80	670	15	23	36	154
100	650	16	24	56	155
120	613	17	24	51	160
140	602	18	24	54	155
160	491	19	24	22	140
180	703	18	23	27	140
200	439	23	24	43	114
220	479	24	26	54	134
240	596	13	24	31	167
260	452	18	24	57	159
280	535	24	26	56	134
300	929	15	20	58	124
320	670	17	23	58	135
340	417	6	21	59	173
360	367	6	22	55	183
380	309	8	20	53	177
400	231	8	22	46	188
420	287	9	20	50	170
440	277	10	21	45	159

APPENDIX C

X-ray Diffractometry Results

Sample	Quartz ¹	Calcite ¹	Smectite ²	Illite ²	Kaolinite ²
MabX 265	X	X	X	X	X
MabX 305	X	-	X	X	X
Mab6 200	X	X	X	X	X
Mab6 320	X	X	X	X	X

¹ Determined from bulk run

² Determined from clay extraction

X Indicates present in sample

- Not detected in sample

VITA

Jennifer L. Gamrod

Candidate for the Degree of

Master of Science

Thesis: PALEOLIMNOLOGICAL RECORDS OF ENVIRONMENTAL CHANGE
PRESERVED IN PALEO-LAKE MABABE, NORTHWEST BOTSWANA

Major Field: Geology

Biographical:

Education:

Completed the requirements for the Master of Science degree in Geology at
Oklahoma State University, Stillwater, Oklahoma in July, 2009.

Completed the requirements for the Bachelor of Science degree in Geology at
Southern Methodist University, Dallas, Texas in December 2005.

Professional Memberships:

American Association of Petroleum Geologists
Geological Society of America

Name: Jennifer Leigh Gamrod

Date of Degree: July 2009

Institution: Oklahoma State University

Location: Stillwater, Oklahoma

Title of Study: PALEOLIMNOLOGICAL RECORDS OF ENVIRONMENTAL
CHANGE PRESERVED IN PALEO-LAKE MABABE, NORTHWEST
BOTSWANA

Pages in Study: 43

Candidate for the Degree of Master of Science

Major Field: Geology

Findings and Conclusions:

Lacustrine sediments preserve a record of environmental change from climate shifts and landscape evolution. Paleo-lake Mababe in northwest Botswana was investigated to determine how the effects of tectonics along the incipient Okavango Rift, as well as local and regional climatic changes are recorded in lake sediments. This multi-proxy study using grain size distribution, magnetic susceptibility, organic and inorganic carbon content, and metal data revealed a major shift in hydrology and sedimentation. The shift is due to tectonic activity associated with movement along faults that diverted river flow away from the Mababe Depression. Sediments deposited prior to tectonic activity show evidence of local and regional climate. Post-tectonic sedimentation revealed local and regional climatic shifts and the new hydrologic regime established by neotectonics. Major reorganization of regional hydrology resulting from tectonic activity in the Okavango rift zone affected sedimentation in lakes in the middle Kalahari in northwest Botswana.

ADVISER'S APPROVAL: Dr. Anna Cruse
